

LEWIS/GRANT/IN-34

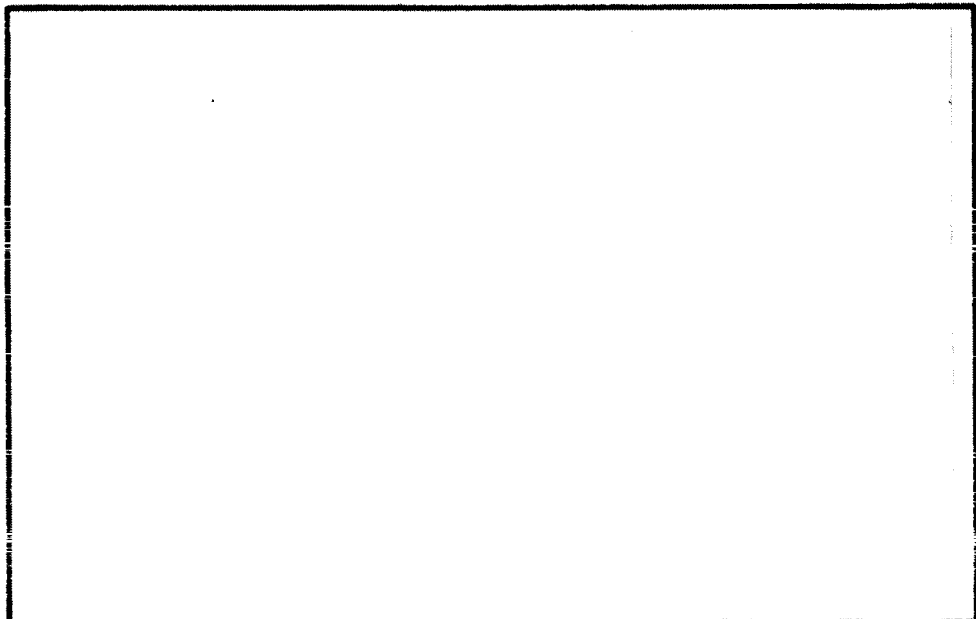
79766-CR

(1+4)

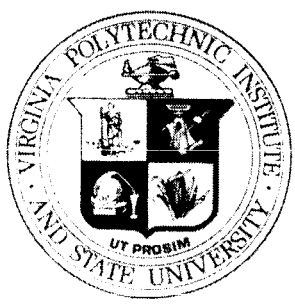
1987-01-180327) THE INSTITUTE OF TECHNOLOGY  
1. National University of Science and Technology  
2. The University of Maryland System, 30 100  
3. The University of Virginia, Charlottesville  
4. The State University of New York at Binghamton  
(187) and State Univ.) 23 p Avail: NIS 83/54 007870

327-2100  
000000  
000000  
000000  
007870

# OF COLLEGE ENGINEERING



# VIRGINIA POLYTECHNIC INSTITUTE AND STATE UNIVERSITY



BLACKSBURG,  
VIRGINIA

Final Report on NASA Grant No. NAG 3-593  
Thermodynamic Evaluation of Transonic Compressor Rotors  
Using the Finite Volume Approach

for the period  
12/20/84 - 12/19/86

by  
John Moore  
Professor of Mechanical Engineering  
Principal Investigator

Stephen Nicholson  
Instructor  
and  
Joan G. Moore  
Research Associate

Grantee Institution -  
NASA Lewis Research Center  
21000 Brookpark Road  
Cleveland, Ohio 44135

Turbomachinery Research Group  
Report No. JM/87-4

Mechanical Engineering Department  
Virginia Polytechnic Institute and State University  
Blacksburg, Virginia 24061

TABLE OF CONTENTS

|  | Page |
|--|------|
| 1. <u>Abstract</u>   | 3    |
| 2. <u>Development of an Explicit Time Marching Procedure<br/>for Laminar and Turbulent Flow</u><br>- Summary Viewgraphs  | 4    |
| 3. <u>List of Project Reports and Papers</u><br>Title Pages and Abstracts of Reports in Appendix A<br>Copies of Papers in Appendices B and C   | 13   |
| 4. <u>Backflow - Extensions to the Computational Procedure</u><br>Discretization of Convection Term<br>Improved Pressure Interpolation for SBLI<br>Evaluation of Turbulent Viscosity | 14   |
| 5. <u>Backflow - Test Cases</u><br>UTRC Separated and Reattached Turbulent Boundary Layer<br>MDRL Diffuser - Strong Shock Case   | 22   |
| 6. <u>Mach Number Dependent Interpolation Formula<br/>for Density-Update Time-Marching Methods</u>   | 35   |
| <br><u>Appendices</u>  |      |
| A. Title Pages and Abstracts of Reports  | 46   |
| B. An Explicit Finite-Volume Time-Marching Procedure<br>for Turbulent Flow Calculations  | 59   |
| C. Explicit Finite-Volume Time-Marching Calculations<br>of Total Temperature Distributions in Turbulent Flow   | 71   |

## 1. ABSTRACT

In this final report, we summarize two years work developing computational capability to handle viscous flow with an explicit time-marching method based on the finite volume approach. For attached flow, our findings have been extensively documented, and our main object in this report is to present extensions to the computational procedure to allow the handling of shock induced separation and large regions of strong backflow. Two test cases are considered, the UTRC separated and reattached turbulent boundary layer and the strong shock case in the MDRL transonic diffuser G. The extended method has worked well on the UTRC flow with a boundary layer blockage of 58 percent and a maximum backflow velocity of 37 percent of the local maximum free-stream velocity. It has also worked well on the MDRL diffuser with a shock Mach number of 1.353 and a maximum backflow velocity of -71.7 m/s.

A Mach number dependent interpolation formula for effective pressure has been developed for use in density-update time-marching methods. This is a parallel development based on our earlier stability analysis which resulted in the M&M interpolation formula for effective density.

N87 - 23926

2. DEVELOPMENT OF AN EXPLICIT TIME MARCHING PROCEDURE

FOR LAMINAR AND TURBULENT FLOW

- SUMMARY VIEWGRAPHS

AN EXPLICIT FINITE-VOLUME TIME-MARCHING PROCEDURE  
FOR TURBULENT FLOW CALCULATIONS

Start: Denton explicit time-marching method.  
Allure - easy to understand method.

Continuity

$$\frac{\partial \rho}{\partial t} + \frac{\partial \rho u}{\partial x} + \frac{\partial \rho v}{\partial y} + \frac{\partial \rho w}{\partial z} = 0$$

$$\delta \rho = \left[ - \frac{\partial \rho u}{\partial x} - \frac{\partial \rho v}{\partial y} - \frac{\partial \rho w}{\partial z} \right] \delta t$$

Momentum

$$\delta(\rho u) = [\text{steady eqn momentum error}] \delta t$$

$$\delta(\rho v) = [ \quad \quad \quad ] \delta t$$

$$\delta(\rho w) = [ \quad \quad \quad ] \delta t$$

Start: Denton explicit time-marching method.

Questions:

1. Is smoothing necessary for convergence of explicit method ?
2. Why, at low Mach numbers, is the CFL criterion used to get the time step for the momentum equations ?  
(  $\delta t = \delta x / [\text{velocity} + \text{speed of sound}]$  )
3. Why not extend the method to laminar and turbulent flow ?  
What are the problems involved ?
4. Why does he use an interpolated pressure in the momentum equation for transonic flow ?  
Can we show why and when it is stable ?
5. How can the method be extended to separated flow ?

ANSWER ----->

Development of Explicit method for calculation of

Inviscid, Laminar or Turbulent Flow

Mach number = 0 to >2.5, including shocks

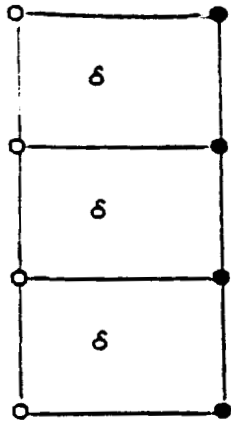
Economical - grid points

With or without separation

Tested on 2-d duct flows



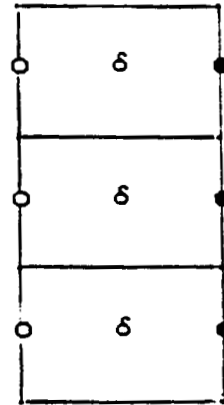
1. Is smoothing necessary for convergence of explicit method ?



Denton control volume  
4 unknowns ●  
3 equations

YES

FLOW  
----->



"New" control volume  
3 unknowns ●  
3 (well-posed) equations

NO

( "New" control volume, traditionally used for boundary layers )

2. Why, at low Mach numbers, is the CFL criterion used to get the time step for the momentum equations ?  
 (  $\delta t = \delta x / [\text{velocity} + \text{speed of sound}]$  )

CONSERVATIVE FORM OF MOMENTUM EQUATION

$$\frac{\partial(\rho u)}{\partial t} + \nabla \cdot \rho \underline{u} u = - \frac{\partial p}{\partial x} + \dots$$

$$u \left[ \frac{\partial \rho}{\partial t} + \nabla \cdot \rho \underline{u} \right] + \rho \frac{\partial u}{\partial t} + \rho \underline{u} \cdot \nabla u = - \frac{\partial p}{\partial x} + \dots$$

continuity

included, therefore  $\delta t_{\text{cont}} = \delta t_{\text{mom}}$   
 Stability analysis, continuity and momentum --->

CFL condition  $\delta t = \delta x / (u+c)$

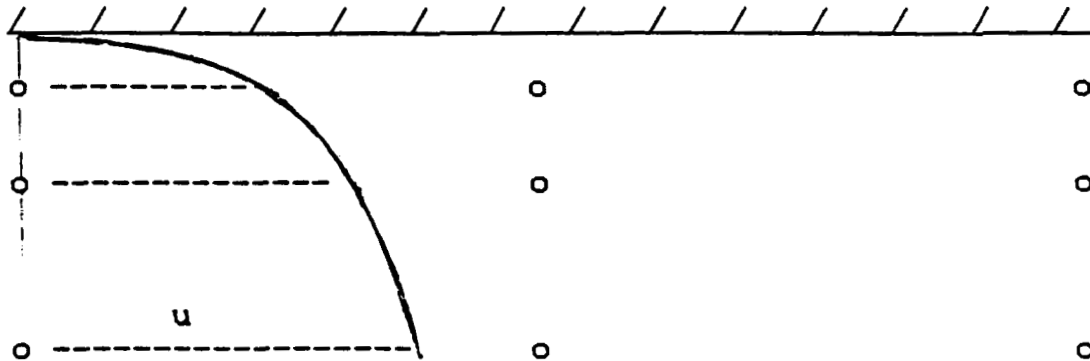
CONVECTIVE FORM OF EQUATION

$$\rho \frac{\partial u}{\partial t} + \rho \underline{u} \cdot \nabla u = - \frac{\partial p}{\partial x} + \dots$$

Stability analysis, momentum equation --->  $\delta t = \delta x / u$

3. Why not extend the method to laminar and turbulent flow ?  
What are the problems involved ?

RESOLUTION OF TRANSVERSE PRESSURE GRADIENT



Flat plate turbulent boundary layer  $\partial p / \partial y \approx 0$

$$p = \rho RT$$

$$\delta p = RT \delta \rho - \frac{\rho R U}{2c_p} \delta U$$

$\delta p$  dependent on continuity and momentum errors -  
stability is highly grid and  $\delta t$  dependent  
difficult without smoothing

Borrow idea from pressure correction methods -  
 $\delta p$  depends only on continuity error.

$$\delta p = RT \delta \rho$$

$$= \left[ \frac{-\partial \rho u}{\partial x} - \frac{\partial \rho v}{\partial y} - \frac{\partial \rho w}{\partial z} \right] RT \delta t$$

Stable without smoothing. Multi-volume approach  
needed for highly nonuniform  $\delta y$  grid spacing.

4. Why does Denton use an interpolated pressure in the momentum equation for transonic flow?  
Can we show why and when it is stable?

Want 
$$\frac{\partial \rho u}{\partial x} + \frac{\partial \rho v}{\partial y} + \frac{\partial \rho w}{\partial z} = 0$$

1-D stability analysis. 
$$\begin{aligned} \rho &= \rho + \delta\rho \\ u &= u + \delta u \\ \delta u &\approx -C \frac{\partial(\delta p)}{\partial x} \\ \delta p &\approx RT \frac{\partial \rho}{\partial x} \end{aligned}$$

Interpolated pressure

$$p_i = (\rho RT)_i \quad \text{or} \quad p_i = .5[(\rho RT)_{i+1} + (\rho RT)_{i-1}] \quad \text{or} \quad \dots$$

----->  

$$A_i \delta\rho_i + A_{i+1} \delta\rho_{i+1} + A_{i-1} \delta\rho_{i-1} + \dots$$

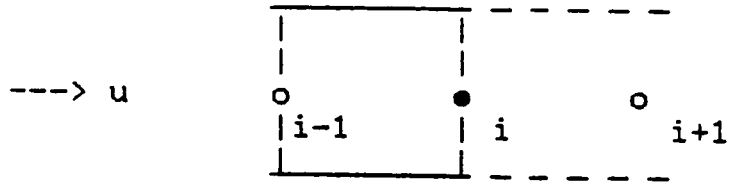
= continuity error, each control volume

Explicit method approximation  
 $[1/\delta t] \delta\rho_i = \text{continuity error for control volume}$

Stability requires  $A_i$  positive and dominant.

5. How can the method be extended to separated flow ?

(a) UPWIND DIFFERENCING



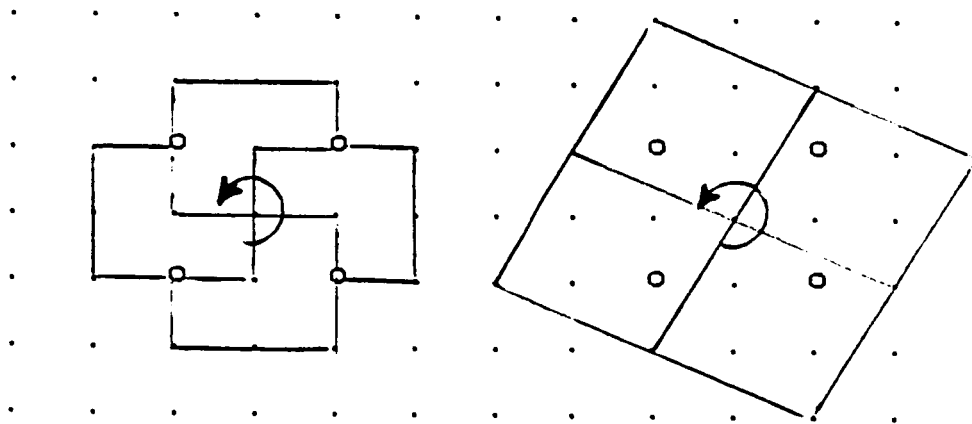
$u > 0 \quad u \frac{\partial u}{\partial x} = u (u_i - u_{i-1}) / \delta x$

$u < 0 \quad u \frac{\partial u}{\partial x} = (-u)(u_i - u_{i+1}) / \delta x$

----> positive coefficient for  $u_i$

(b) UPWINDED CONTROL VOLUMES

- control volumes depend on local  $u$



----> positive coefficient for  $u_i$

### 3. LIST OF PROJECT REPORTS AND PAPERS

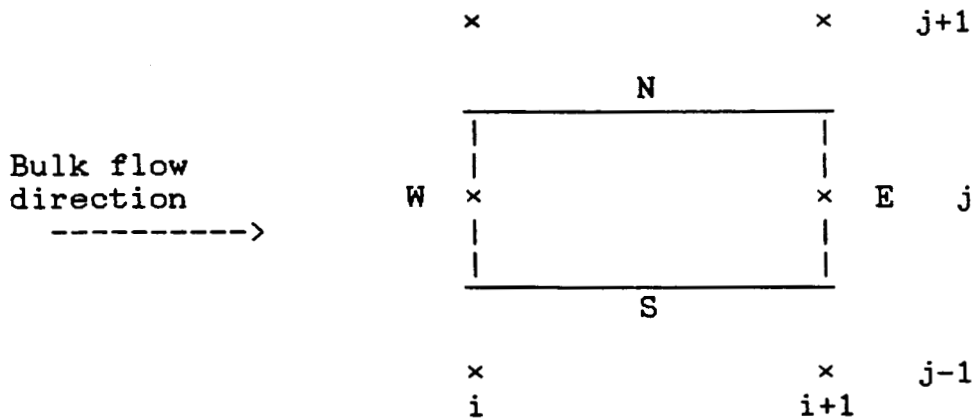
1. Nicholson, S., "Development of a Finite Volume Time Marching Method," Turbomachinery Research Group Report No. JM/85-3, Mechanical Engineering Dept., VPI&SU, February 1985.
2. Nicholson, S., and Moore, J., "Semi-Annual Status Report on NASA Grant No. NAG 3-593 for the Period 12/20/84 - 5/31/85," Turbomachinery Research Group Report No. JM/85-6, Mechanical Engineering Dept., VPI&SU, June 1985.
3. Moore, J., Nicholson, S., and Moore, J.G., "Annual Report on NASA Grant No. NAG 3-593 for the Period 12/20/84 - 12/19/85," Turbomachinery Research Group Report No. JM/85-11, Mechanical Engineering Dept., VPI&SU, December 1985.
4. Nicholson, S., and Moore, J., "Semi-Annual Status Report on NASA Grant No. NAG 3-593 for the Period 12/20/85 - 5/31/86," Turbomachinery Research Group Report No. JM/86-2, Mechanical Engineering Dept., VPI&SU, June 1986.
5. Nicholson, S., "Extension of the Finite Volume Method to Laminar and Turbulent Flow," Ph. D. Dissertation and Turbomachinery Research Group Report No. JM/86-6, Mechanical Engineering Dept., VPI&SU, August 1986.
6. Nicholson, S., Moore, J.G., and Moore, J., "An Explicit Finite-Volume Time-Marching Procedure for Turbulent Flow Calculations," 5th International Conference on Numerical Methods in Laminar and Turbulent Flow, Montreal, Canada, July, 1987.
7. Nicholson, S., Moore, J.G., and Moore, J., "Explicit Finite-Volume Time-Marching Calculations of Total Temperature Distributions in Turbulent Flow," 5th International Conference on Numerical Methods in Laminar and Turbulent Flow, Montreal, Canada, July, 1987.

#### 4. BACKFLOW - EXTENSIONS TO THE COMPUTATIONAL PROCEDURE

##### 4a. Discretization of Convection Terms

The momentum and energy equations are discretized over control volumes fixed relative to the grid points. Central differencing is used except in regions where there are large cross flows or backflow. In these regions a side upwind or reverse upwind differencing is used for stability. The details are as follows.

Control volume for momentum or energy for point  $i+1, j$ .



Convection of property  $\phi$  where

$\phi = u$  for x-momentum

$\phi = v$  for y-momentum

$\phi = h$  for energy (enthalpy) equation.

Convection term integrated over control volume

$$\begin{aligned} \int \rho \underline{u} \cdot \nabla \phi \, dVol &= \int \nabla \cdot \rho \underline{u} \phi \, dVol - \phi_M \int \nabla \cdot \rho \underline{u} \, dVol \\ &= \oint \phi \rho \underline{u} \cdot d\Delta - \phi_M \oint \rho \underline{u} \cdot d\Delta \\ &= (\rho \underline{u} \cdot \Delta)_N \phi_N + (\rho \underline{u} \cdot \Delta)_S \phi_S + (\rho \underline{u} \cdot \Delta)_E \phi_E + (\rho \underline{u} \cdot \Delta)_W \phi_W \\ &\quad - \phi_M [(\rho \underline{u} \cdot \Delta)_N + (\rho \underline{u} \cdot \Delta)_S + (\rho \underline{u} \cdot \Delta)_E + (\rho \underline{u} \cdot \Delta)_W] \end{aligned}$$

We wish to express this in terms of the  $\phi$ 's at the grid points, i.e we want the equation in the form

$$\begin{aligned} \int \rho \underline{u} \cdot \nabla \phi \, dVol &= C_E \phi_{i+1, j} + C_W \phi_{i, j} + C_{EE} \phi_{i+2, j} \\ &\quad + C_{NE} \phi_{i+1, j+1} + C_{NW} \phi_{i, j+1} + C_{SE} \phi_{i+1, j-1} + C_{SW} \phi_{i, j-1} \end{aligned}$$

The coefficients C are determined from the mass fluxes through the sides  $(\rho \underline{u} \cdot \Delta)$  and the discretization choice for  $\phi_N$ ,  $\phi_S$ ,  $\phi_E$ ,  $\phi_W$ , and  $\phi_M$ .

For stability we wish the center point coefficient,  $C_E$ , to be positive and greater than the sum of the other positive coefficients.

$$\underline{\phi_M}$$

When  $[(\rho \underline{u} \cdot \Delta)_N + (\rho \underline{u} \cdot \Delta)_S + (\rho \underline{u} \cdot \Delta)_E + (\rho \underline{u} \cdot \Delta)_W] > 0$

take  $\phi_M = \phi_{i,j}$

to give a negative contribution to  $C_W$ .

When  $[(\rho \underline{u} \cdot \Delta)_N + (\rho \underline{u} \cdot \Delta)_S + (\rho \underline{u} \cdot \Delta)_E + (\rho \underline{u} \cdot \Delta)_W] < 0$

take  $\phi_M = \phi_{i+1,j}$

to give a positive contribution to  $C_E$ .

$$\underline{\phi_E \text{ and } \phi_W}$$

When  $(\rho \underline{u} \cdot \Delta)_E > 0$

$$\phi_E = \phi_{i+1,j}$$

This centered evaluation of  $\phi_E$  (second order accurate) gives a positive contribution to  $C_E$ .

When  $(\rho \underline{u} \cdot \Delta)_E < 0$

$$\phi_E = \phi_{i+2,j}$$

This upwind evaluation of  $\phi_E$  (first order accurate) gives a negative contribution to  $C_{EE}$ .

This also determines  $\phi_W$  since  $\phi_E$  for one control volume is  $\phi_W$  for the next control volume.

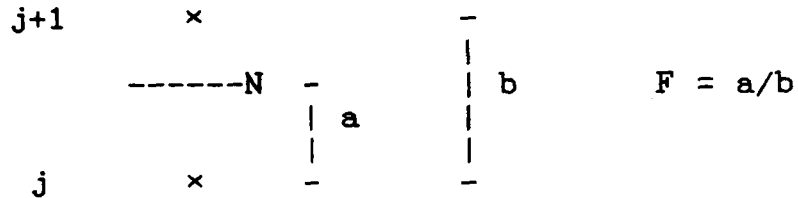


$\phi_N$  and  $\phi_S$

The geometrical centered evaluation for  $\phi_N$  is

$$\phi_N = 0.5 [(1-F)(\phi_{i+1, j} + \phi_{i, j}) + F(\phi_{i+1, j+1} + \phi_{i, j+1})]$$

where F is the fraction of the distance of the North face between the grid points.



For accuracy this centered evaluation should be used whenever possible.

For stability when

$$(\rho \underline{u} \cdot \Delta)_N > 0 \text{ and } (\rho \underline{u} \cdot \Delta)_E > 0$$

take  $F \leq (\rho \underline{u} \cdot \Delta)_E / (\rho \underline{u} \cdot \Delta)_N$

When the inequality is chosen, which for equal grid spacing will occur when  $(\rho \underline{u} \cdot \Delta)_N > 2(\rho \underline{u} \cdot \Delta)_E$ ,

$$\begin{aligned} (\rho \underline{u} \cdot \Delta)_N \phi_N &= 0.5(\phi_{i+1, j} + \phi_{i, j}) [(\rho \underline{u} \cdot \Delta)_N - (\rho \underline{u} \cdot \Delta)_E] \\ &\quad + 0.5(\phi_{i+1, j+1} + \phi_{i, j+1}) (\rho \underline{u} \cdot \Delta)_E \end{aligned}$$

When  $(\rho \underline{u} \cdot \Delta)_N > 0$  and  $(\rho \underline{u} \cdot \Delta)_E \leq 0$

(the primary flow is locally backwards or zero relative to the bulk flow direction)

take  $\phi_N = \phi_{i+1, j}$

By symmetry for  $(\rho \underline{u} \cdot \Delta)_S > 0$  and  $(\rho \underline{u} \cdot \Delta)_E > 0$

take  $F \geq 1 - (\rho \underline{u} \cdot \Delta)_E / (\rho \underline{u} \cdot \Delta)_S$

and  $\phi_S = 0.5[(1-F)(\phi_{i+1, j-1} + \phi_{i, j-1}) + F(\phi_{i+1, j} + \phi_{i, j})]$

For  $(\rho \underline{u} \cdot \Delta)_S > 0$  and  $(\rho \underline{u} \cdot \Delta)_E \leq 0$

take  $\phi_S = \phi_{i+1, j}$ .

When  $(\rho u \cdot \Delta)_N$  is negative,  $(\rho u \cdot \Delta)_S$  is positive for the next, the  $j+1$ , control volume, so that  $\phi_N$  is determined from  $\phi_S$  for the  $j+1$  control volume. Similarly when  $(\rho u \cdot \Delta)_S$  is negative,  $\phi_S$  is determined from  $\phi_N$  for the  $j-1$  control volume.

Comparison with earlier scheme.

In these terms, Nicholson (Section 3, Report 5, JM/86-6) considered only positive values for  $(\rho u \cdot \Delta)_E$ , i.e. no reverse flow. The formulae he used for  $\phi_M$ ,  $\phi_E$  and  $\phi_W$  were the same as given here. However the upwinding he took for the cross flows was different. In particular when  $(\rho u \cdot \Delta)_N$  was positive,  $\phi_N$  was evaluated using

$$F \leq \frac{1}{3} (\rho u \cdot \Delta)_E(\text{at } i-1) / (\rho u \cdot \Delta)_N + \frac{1}{3}$$

Taking  $F \leq (\rho u \cdot \Delta)_E / (\rho u \cdot \Delta)_N$  gives lower and hence more conservative values of  $F$  when  $(\rho u \cdot \Delta)_N > 2(\rho u \cdot \Delta)_E$ , i.e., where for uniform grid spacing, the geometric  $F$  may not be used.

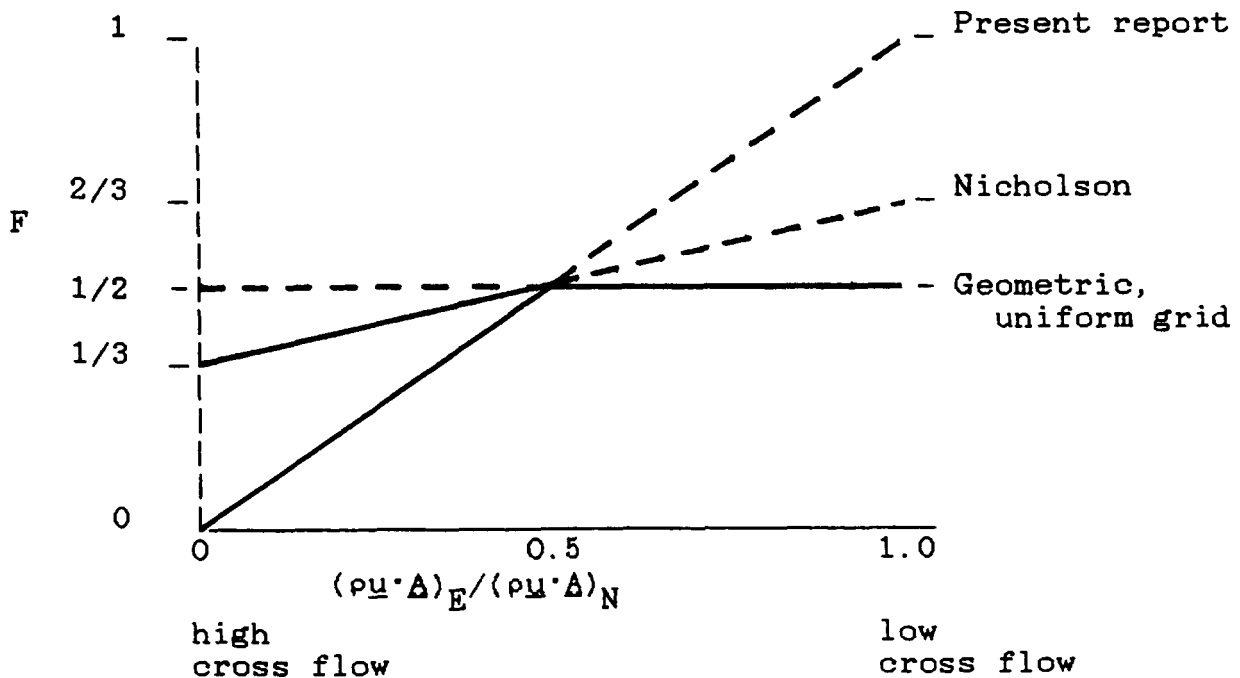

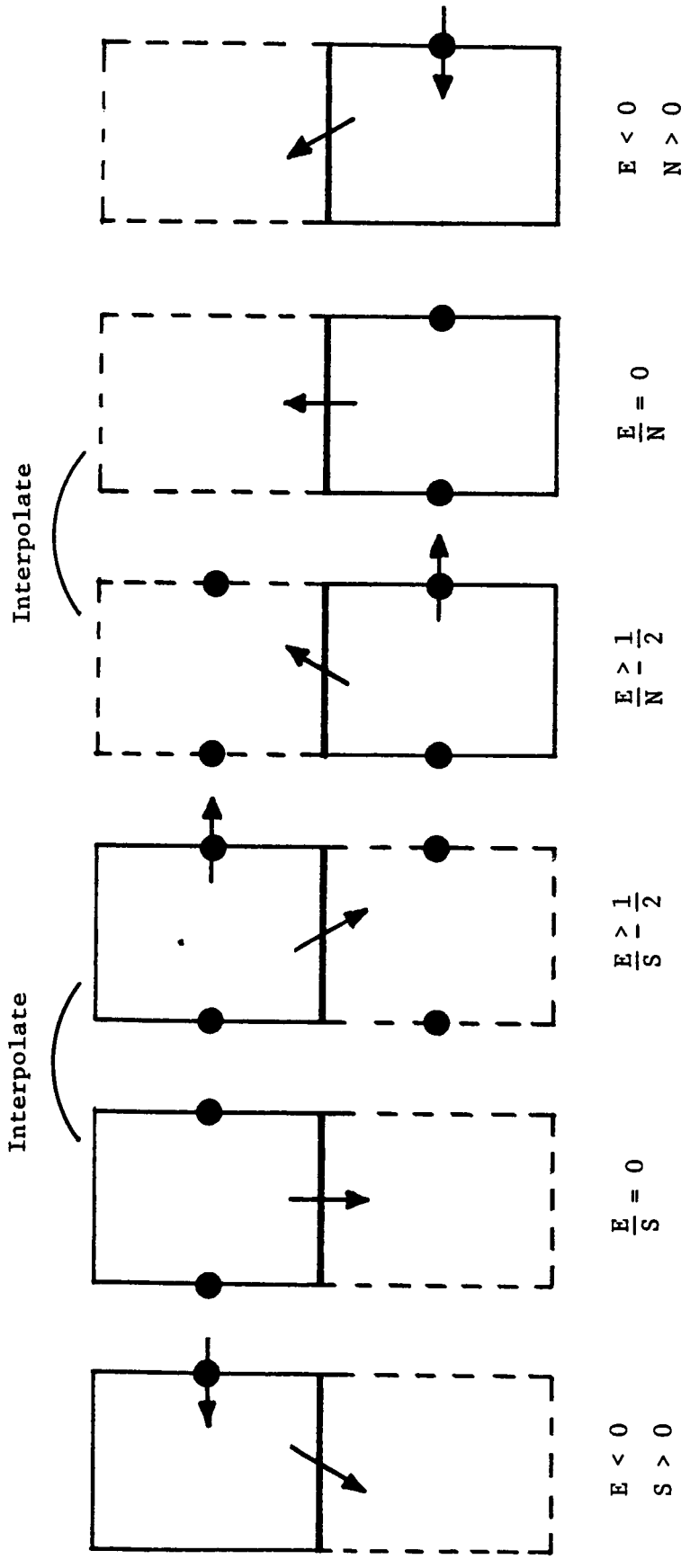
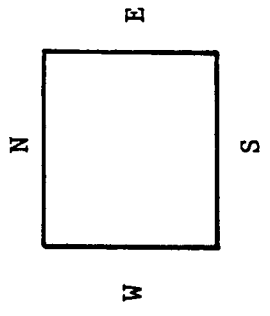


Table 1 SIDE UPWINDING ALGORITHM -  
Summary for Uniform Grid Spacing

For side , convected property = average of points marked  .



Bulk flow direction



Mass fluxes: N, S, E, W



#### 4c. Evaluation of Turbulent Viscosity for the Present Test Cases

The turbulence model used in the calculations is a Prandtl mixing length formulation

$$\mu_t = \rho L^2 "du/dy"$$

where the mixing length L is the smaller of

$$\begin{aligned} & 0.41y \text{ (with a Van Driest correction)} \\ \text{or } & 0.08\delta. \end{aligned}$$

Sometimes it is difficult to determine an appropriate boundary layer thickness,  $\delta$ .

For the present test cases

- (a) UTRC, boundary layer separation geometrically triggered and
- (b) Sajben diffuser, separation induced by shock,

the boundary layer thickness used to calculate L was changed to obtain a reasonable separation when compared with the measurements. The details of what was used to determine the effective boundary layer thickness follow.

##### Determining the edge of the boundary layer.

The location of the edge of the boundary layer is determined by the total pressure gradient  $|dp_t/dy|$ . In particular a search starts from outside the boundary layer (in the middle of the duct) and proceeds towards the wall to locate where

$$\left| \frac{dp_t}{dy} \right| = \frac{(p_o - p) *DPFACT}{(\text{local duct width})}$$

This is the edge of the boundary layer for the mixing length calculation. The larger the DPFACT the smaller the boundary layer thickness.

| Case                          | DPFACT |
|-------------------------------|--------|
| (a) UTRC, sep. b.l.           | 2.0    |
| (b) Sajben, $p_e/p_o = 0.722$ | 2.5    |

"Time" lag for boundary layer thickness.

For case (b), Sajben  $p_e/p_o = 0.722$ , shrinking  $\delta$  by increasing DPFAC was insufficient to correctly obtain the separation induced by the shock. Qualitatively since turbulence is convected with the flow there needs to be time for the turbulence to change - it does not change suddenly. This was qualitatively introduced into the calculation by lagging the boundary layer thickness used for the calculation of L by 5 grid points. (The lag is between 0.5 and 0.75 throat heights through the separation region.) In particular after  $i = 40$  ( $x/h=1.7$ , upstream of the shock at  $x/h \approx 2.4$  but well downstream of the throat at  $x/h=0$ ) the mixing length in the outer part of the boundary layer was obtained using

$$L(i) = 0.08\delta(i-5).$$

The time lag was used only for case (b).

## 5. BACKFLOW - TEST CASES

The extensions to the computational procedure described in section 4 were necessary for modelling two extreme cases of separated flow, the UTRC separated and reattached flat plate turbulent boundary layer (NASA Contract NAS3-22770, reference 1) and the MDRL transonic diffuser flow with a strong shock (MDRL Report No. 81-07, reference 2). These cases exhibit large boundary layer blockage (displacement thickness/local duct height), large backflow velocities, relative to the free stream velocity, and high rms/mean turbulence levels in the backflow region. The maximum boundary layer blockages were 58 percent (fifty eight!) in the UTRC low speed ( $U_{ref} = 27$  m/s) flow and 27 percent in the MDRL diffuser with a shock Mach number of 1.353. The maximum backflow velocities were 37 percent and 25 percent, respectively, of the local maximum free-stream velocity. The ratios of rms/mean axial velocities at the locations of maximum reverse flow velocity were 35 percent in the UTRC flow and 66 percent in the MDRL diffuser. If the backflows in the two cases were varying sinusoidally, these values would correspond to maximum backflow velocities of  $-5.4 \pm 2.7$  m/s and  $-71.7 \pm 67.3$  m/s, respectively.

### UTRC Separated and Reattached Turbulent Boundary Layer

The geometry and streamlines for flow through the UTRC test section are shown in Fig. 1; and laser doppler velocity measurements are shown in Fig. 2. The corresponding calculated velocity vectors together with the locus of points for which  $U=0$  are seen in Fig. 3. The size of the reverse flow region is well modelled, and the maximum calculated reverse flow velocity of  $-4.1$  m/s agrees well with the measured maximum value of  $-5.4$  m/s. This good agreement for the reverse flow leads to reasonable agreement between the measured and calculated values of skin friction coefficient in the separation zone, as shown in Fig. 4. The calculated locations of separation and reattachment are seen to be close to the measured locations. The good agreement in the separated flow region was obtained with the Prandtl mixing length model by reducing the turbulent viscosity in the boundary layer as discussed in section 4 (i.e. by using  $DPFACT = 2.0$ ). This then gave a corresponding decrease in the calculated skin friction upstream and downstream of the separation zone, as seen in Fig. 4. We conclude that the present explicit computational procedure can be used for flows with extensive and strong backflow but that a more sophisticated turbulence model is required.

## MDRL Diffuser - Strong Shock Case

With a back pressure,  $p_{\text{exit}}/p_{0,\text{inlet}}$ , of 0.722, the MDRL diffuser G had a shock Mach number of 1.353. Shock induced separation occurred in the turbulent boundary layer on the curved top wall. This contrasts with the case of 0.805 pressure ratio which gave a shock Mach number of 1.235 and no separation. In this section, results of calculations for these two flows will be compared, with particular attention being given to the backflow in the strong shock case.

The calculated shock locations are clearly seen for the two cases in the contours of static pressure in Fig. 5. The strong shock is located further downstream and shows evidence of a lambda foot at the curved top wall. The computed shocks are both quite sharp as a result of the use of the M&M pressure interpolation formula (see section 3 of this report, reference 3).

For the strong shock case, the computed and measured static pressure distributions on the top wall are compared in Fig. 6. The computed shock is just downstream of the measured location and is therefore somewhat stronger with a shock Mach number of 1.39. Upstream of the shock the static pressures are indistinguishable; but downstream the calculated static pressures are consistently higher than those measured, perhaps partly because of three-dimensionality in the measured flow.

The Mach number contours in Fig. 7 show the flow accelerating up to the shock and decelerating downstream. The top wall boundary layer thickens appreciably more through the strong shock. This is seen also in the velocity vectors of Fig. 8, which show the separation bubble downstream of the strong shock. Fig. 9 shows this calculated backflow in more detail, and for comparison the magnitude and possible variations of the measured backflow are also shown. The maximum calculated backflow velocity of -87.7 m/s agrees quite well with the maximum measured value of -71.7 m/s.

Figures 8 and 9 demonstrate quite graphically the significant blockage caused by the separation bubble; and this is also seen in Fig. 10, which shows contours of total pressure.

We conclude that calculations of diffuser flows with strong shocks and shock induced separation can be performed with the present explicit method. As discussed in section 4, this calculation required a time lag of the turbulent viscosity to give a reduced viscosity in the separation bubble. In fact, this simple modification to the turbulence model produced a dramatic upstream movement of the shock and the calculation rapidly converged on a shock location close to that measured. Again this suggests the need for a more sophisticated turbulence model. But the present study of strong backflows has clearly demonstrated that they can



be modelled with an explicit method based on the finite volume approach.

#### References

1. Patrick, W.P., "Flowfield Measurements in a Separated and Reattached Flat Plate Turbulent Boundary Layer," NASA Contract No. NAS3-22770, Draft Final Report, August 1985.
2. Salmon, J.T., Bogar, T.J., and Sajben, M., "Laser Velocimeter Measurements in Unsteady, Separated, Transonic Diffuser Flows," AIAA Paper No. 81-1197 (1981). Accepted for publication in AIAA Journal.

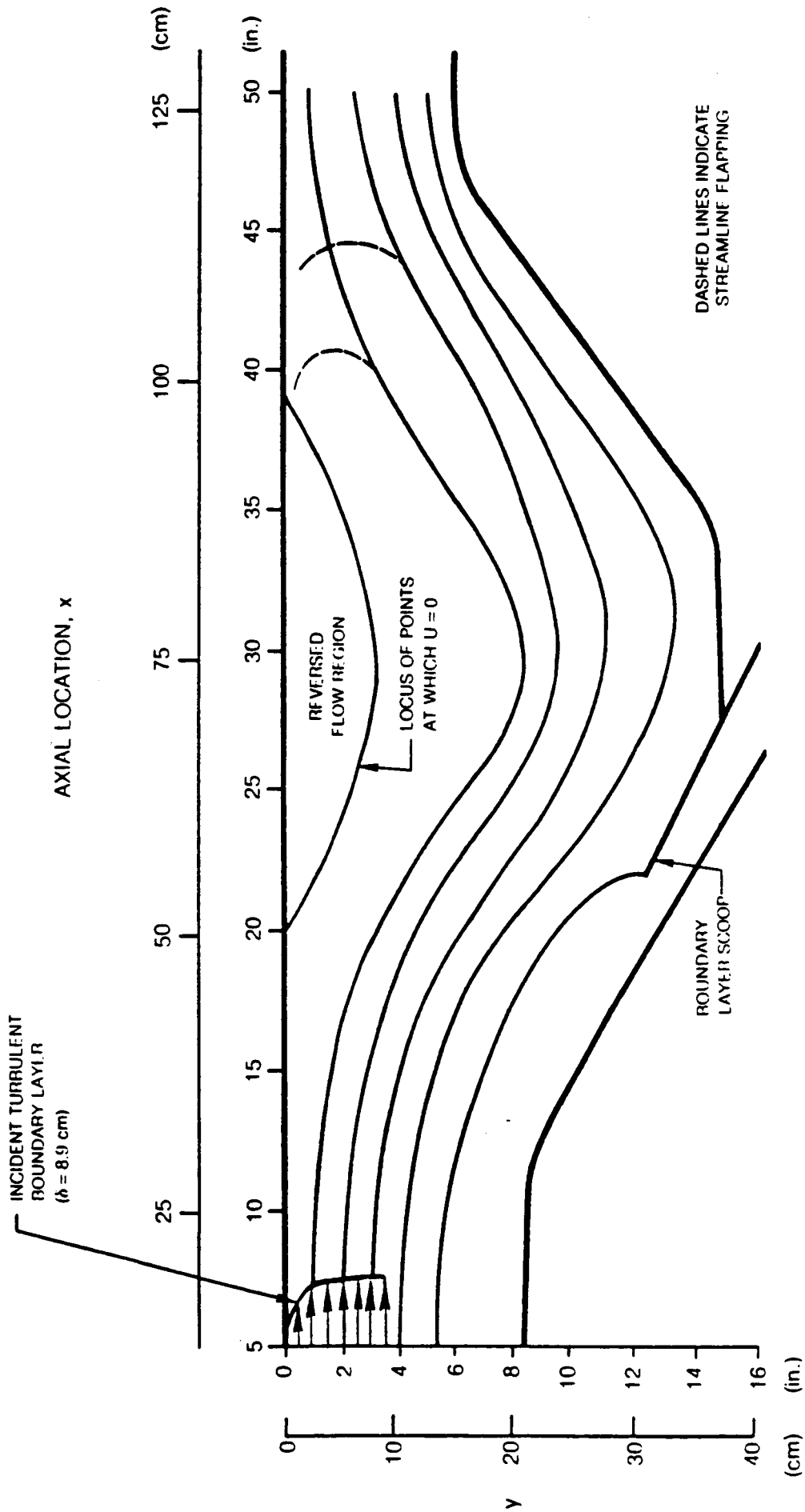


Fig. 1 Streamlines Determined from Smoke Flow Visualization and Tuft Trees (after Patrick [1])

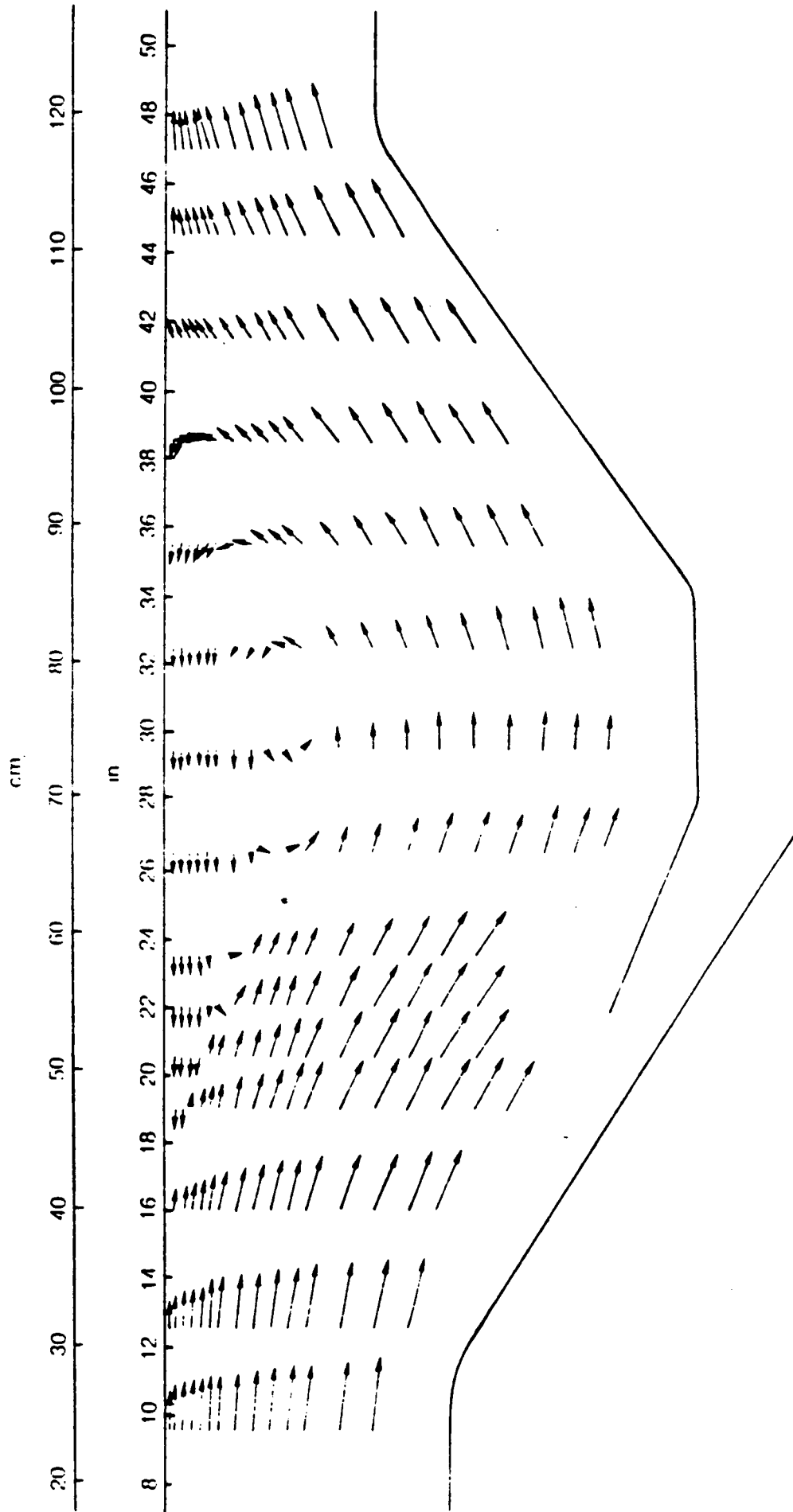


Fig. 2 LV Mean Velocity Measurements on Wind Tunnel Centerline (after Patrick [1])

UTRC SEP. B.L.  
U=0



UTRC SEP. B.L.

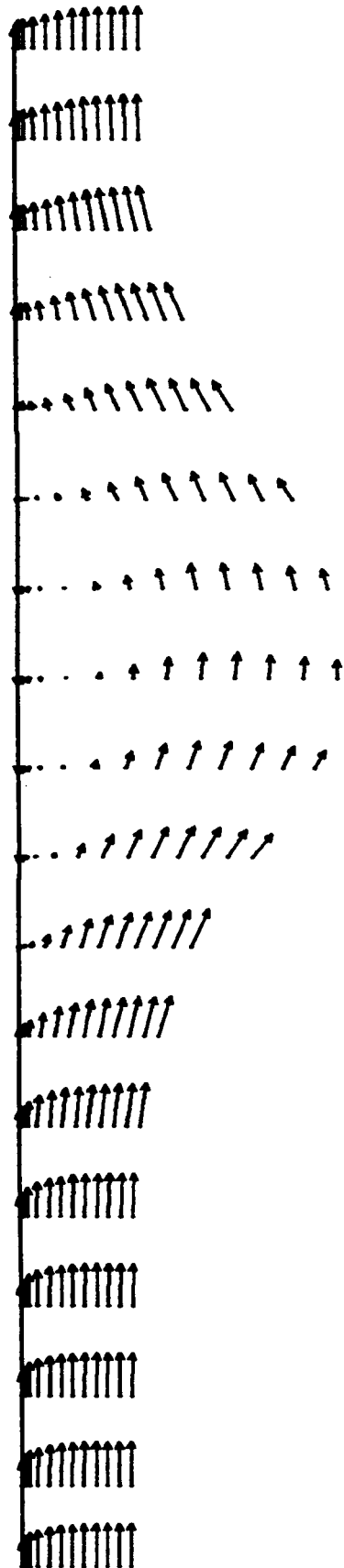


Fig. 3 Calculated velocity vectors and the locus of points for which  $U = 0$ .

| MEASUREMENT METHOD | CALCULATION METHOD |
|--------------------|--------------------|
| ○                  | LAW-WALL           |
| △                  | FOX                |
| □                  | LAW-WALL           |

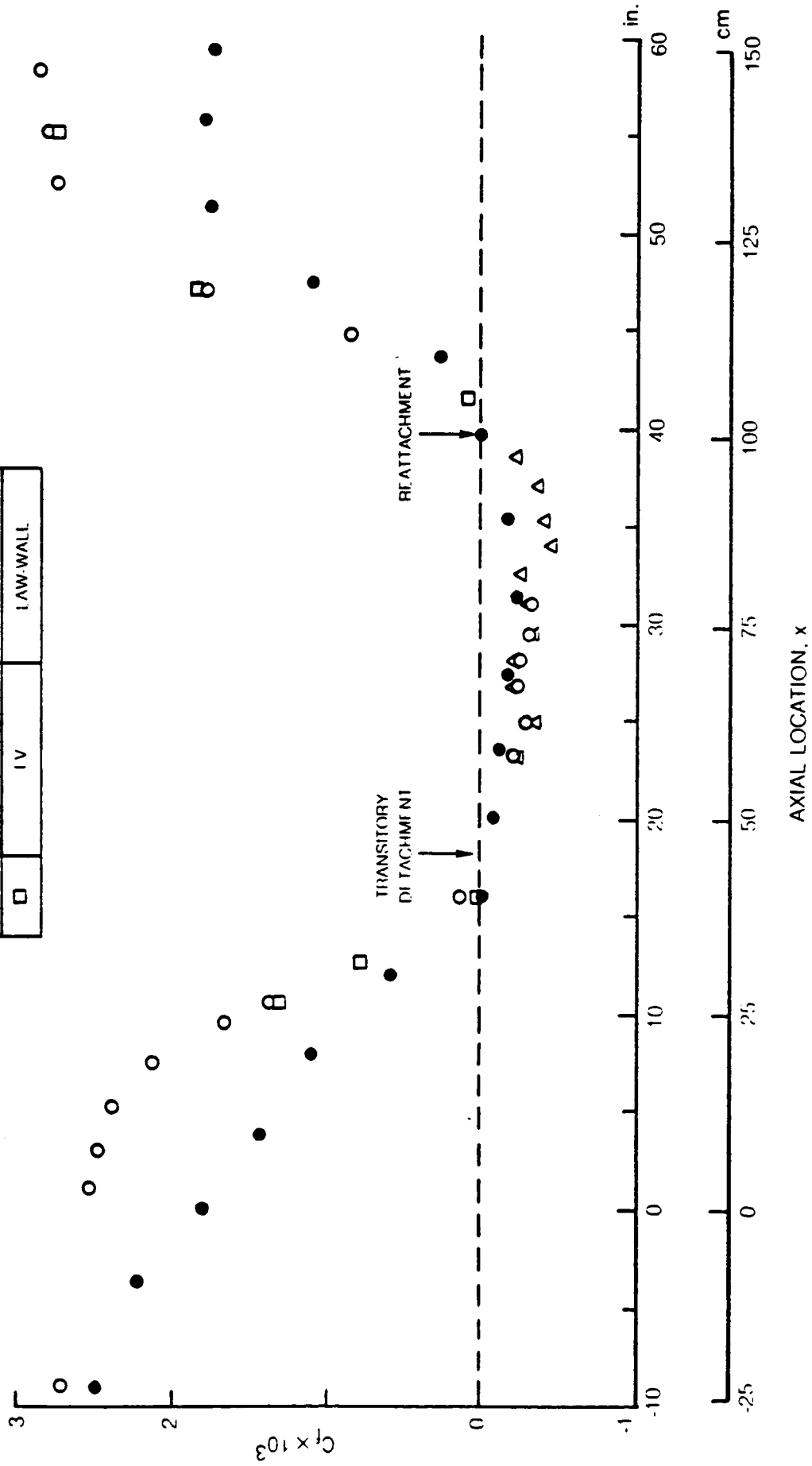
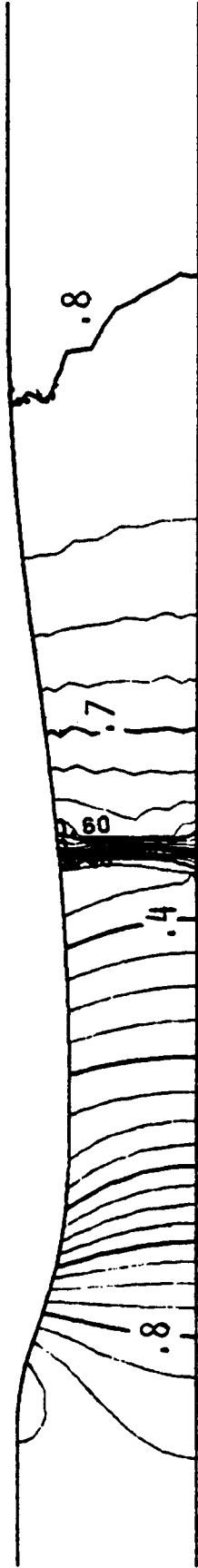


Fig. 4 Skin Friction Coefficient on Test Surface ( $z=0$ , after Patrick [1]). Comparison of calculation results and measurements.

$P_{EXIT}/P_0 = 0.805$



$P_{EXIT}/P_0 = 0.722$



Fig. 5 SAJBEN TRANSONIC DIFFUSER STATIC PRESSURE,  $P/P_0$ , CONTOUR INTERVAL = 0.025

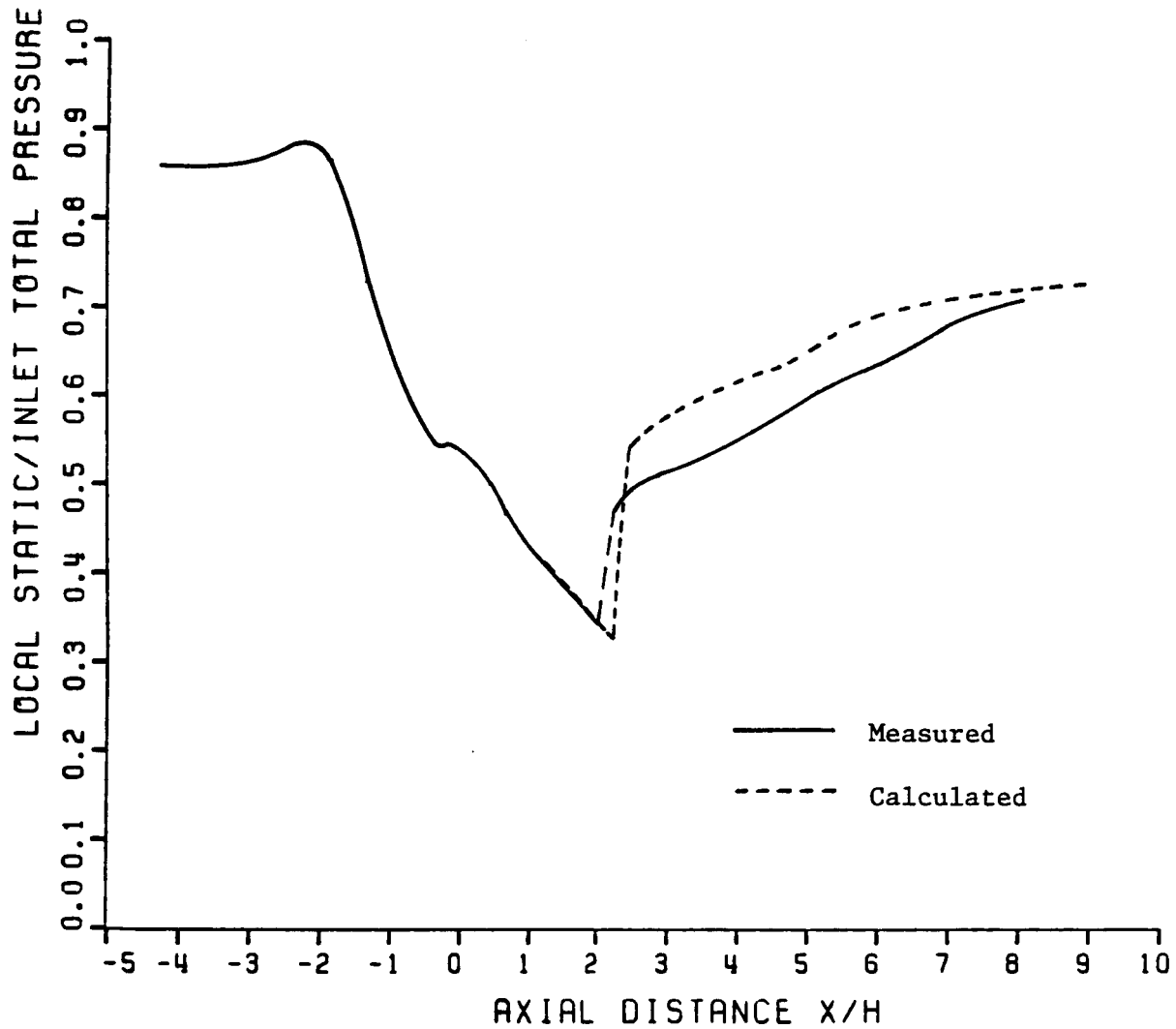


Fig. 6 Computed and measured static pressure distributions on the curved top wall of the MDRL diffuser. Strong shock case;  $p_{\text{exit}}/p_{0\text{inlet}} = 0.722$ .

$$P_{EXIT}/P_0 = 0.805$$



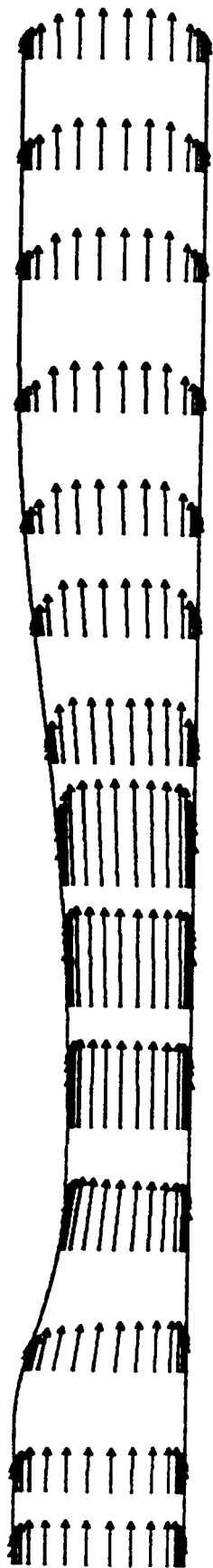
$$P_{EXIT}/P_0 = 0.722$$



Fig. 7 SAJBEN TRANSONIC DIFFUSER MACH NUMBER, CONTOUR INTERVAL = 0.05



$$P_{\text{EXIT}}/P_0 = 0.805$$



$$P_{\text{EXIT}}/P_0 = 0.722$$

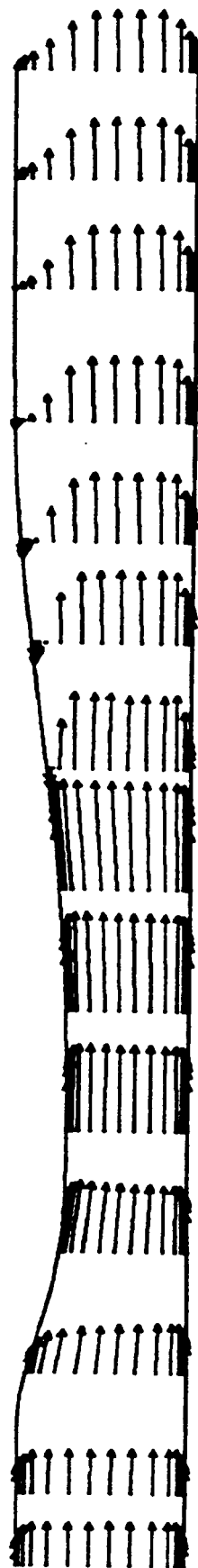


Fig. 8 SAJBEN TRANSONIC DIFFUSER CALCULATED VELOCITY VECTORS

SAJBEN PE/P0 = 0.722

Largest Measured Backflow

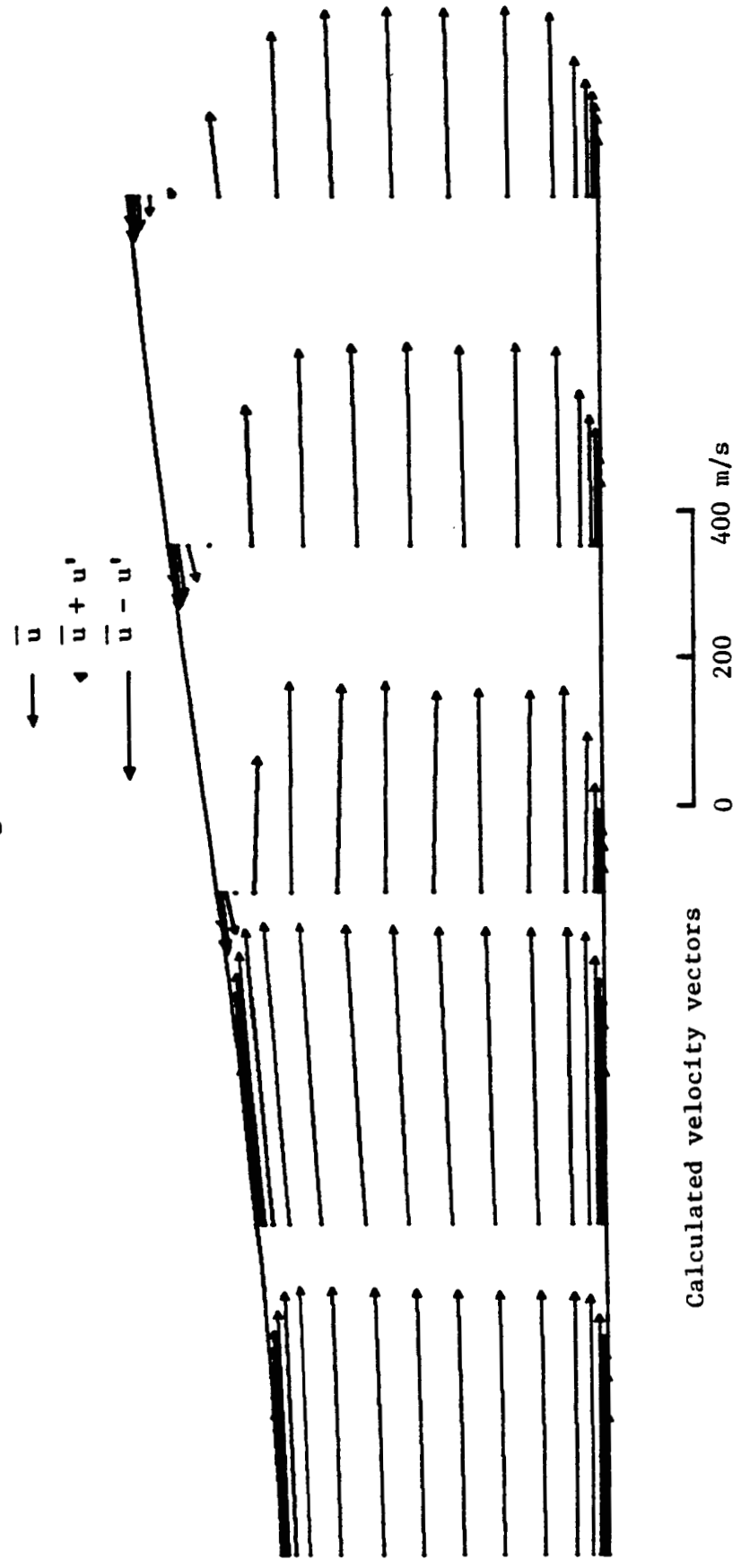


Fig. 9 Calculated velocity vectors upstream of and within the separation bubble.

$$P_{\text{EXIT}}/P_0 = 0.805$$



$$P_{\text{EXIT}}/P_0 = 0.722$$

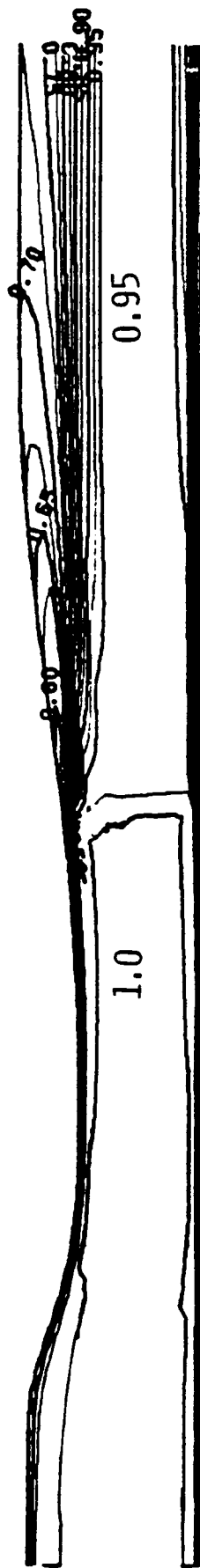


FIG. 10 SAJBEN TRANSONIC DIFFUSER TOTAL PRESSURE,  $P_T/P_0$ , CONTOUR INTERVAL = 0.025

## 6. MACH NUMBER DEPENDENT INTERPOLATION FORMULA FOR DENSITY-UPDATE TIME-MARCHING METHODS

A 1-d stability analysis of density-pressure relations used in the computation of transonic flow was performed in Report No. JM/85-11 (see section 3 of this report, reference 3). Here we give a parallel development of a density interpolation equation for effective pressure for use in density-update methods. The formulae considered are tested using the density-update scheme outlined in Table 1.

### Downwind Effective Pressure

In section 2.8 of reference 3, we considered an inconsistency in the pressure-density relation such that the pressure used in the momentum equation is offset by one grid point from the density used in the continuity equation, i.e.

$$P_i = \rho_{i+1} RT. \quad (40)$$

In a density update method this may be viewed as an effective pressure evaluated downwind of its point of use in the momentum equations. This pressure-density relation was found to be stable for all Mach numbers, but it results in poor shock capturing as the calculated shock is spread over numerous grid points. Fig. 1 shows the calculated and theoretical pressure distributions for a 1-d calculation with a nominal shock number of 1.45.

### Mach Number Dependent Interpolation Formula for Effective Pressure

In section 2.6 of reference 3, we saw that when the Mach number is high, the density update method is stable with the ideal gas equation of state satisfied at each grid point, i.e.,

$$P_i = \rho_i RT_i \quad (73)$$

Since this is the correct pressure-density relation for ideal gases it should be used where feasible. In this section, we will start with a generalized density interpolation equation for effective pressure

$$\rho_i^e = \rho_{i+1} + a_0(\rho_i - \rho_{i+1}) + \frac{a_1}{2}(\rho_i - \rho_{i+2}) + \frac{a_2}{3}(\rho_i - \rho_{i+3}) \quad (74)$$

with 
$$P_i = \rho_i^e RT_i \quad (75)$$

$$\text{and} \quad a_0 + a_1 + a_2 = 1 \quad (76)$$

for second order accuracy.

We seek Mach number limitations to  $a_0$ ,  $a_1$  and  $a_2$  using the stability criterion that

the center point coefficient must be greater than the sum of the other positive coefficients,

$$\text{Coef}_{\text{center}} > \text{Sum Coef}_+ \quad (46)$$

Substituting

$$\frac{\delta p_i}{RT} = \left( a_0 + \frac{a_1}{2} + \frac{a_2}{3} \right) \delta p_i + (1 - a_0) \delta p_{i+1} - \frac{a_1}{2} \delta p_{i+2} - \frac{a_2}{3} \delta p_{i+3} \quad (77)$$

into Eq. 25 of reference 3 and rearranging in terms of the coefficients of each  $\delta p_i$ ,  $a_0$ ,  $a_1$ , and  $a_2$ , yields (neglecting variations of A, u and c with i)

$$\begin{aligned} \frac{Ac}{\delta(M+1)} \{ & \left( \frac{1}{3} a_2 \right) \delta p_{i+4} \\ & \left( \frac{1}{2} a_1 - \frac{2}{3} a_2 \right) \delta p_{i+3} \\ & \left( -1 + a_0 - a_1 + \frac{1}{3} a_2 \right) \delta p_{i+2} \\ & \left( 2 + M\delta(M+1) - 3a_0 - \frac{1}{3} a_2 \right) \delta p_{i+1} \\ & \left( -1 - M\delta(M+1) + 3a_0 + a_1 + \frac{2}{3} a_2 \right) \delta p_i \\ & \left( -a_0 - \frac{1}{2} a_1 - \frac{1}{3} a_2 \right) \delta p_{i-1} \} \\ & = \dot{m}_{\text{change}, i} \quad (78) \end{aligned}$$

Now let us consider a simple second order scheme with  $a_2 = 0$  and  $a_1 = 1 - a_0$ , and find limiting values of  $a_0$ . From Eq. 74, it is obvious that we should consider only values in the range

$$0 \leq a_0 \leq 1. \quad (79)$$

In this range, the coefficient of  $\delta\rho_{i+3}$  is positive or zero, and for the coefficient of  $\delta\rho_{i+1}$  (the center point) to be greater than the coefficient of  $\delta\rho_{i+3}$ , we require

$$a_0 < \frac{3}{5} + \frac{2}{5} M\kappa(M+1). \quad (80)$$

The coefficient of  $\delta\rho_i$  is positive when

$$2a_0 - M\kappa(M+1) > 0 \quad \text{or} \quad M(M+1) < 2a_0/\kappa. \quad (81)$$

In this region, from Eq. 46, we require

$$2 + M\kappa(M+1) - 3a_0 > \frac{1}{2} - \frac{a_0}{2} + 2a_0 - M\kappa(M+1) \quad (82)$$

or

$$a_0 < \frac{1}{3} + \frac{4}{9} M\kappa(M+1). \quad (83)$$

This criterion is more restrictive than Eq. 80 and the corresponding stability limit is shown as a function of Mach number in Fig. 2 for the conservative case of  $\kappa = 1.0$ .

A set of equations for  $a_0$ ,  $a_1$  and  $a_2$ , which satisfy the stability criteria (Eqs. 80 and 83) and give second order accurate interpolation (Eq. 76) has been selected; that is

$$\begin{aligned} a_0 &= \frac{4}{9} M(M+1) \\ a_1 &= 1 - a_0 \\ a_2 &= 0. \end{aligned} \quad (84)$$

This Mach number dependent formulation for  $a_0$  and  $a_1$  is shown in Fig. 3. These equations are referred to as the M&M Mach number dependent interpolation formula for density-update time-marching methods.

## Computational Tests of the M&M Density Interpolation Formula

In this section, results of shock capturing with the M&M formula (Eq. 84) in the density update method (Table 1) are presented for Denton's 1-d nozzle.

### Calculation Details

|                                      |            |                          |
|--------------------------------------|------------|--------------------------|
| Number of axial grid points          | = 46,      | $\delta x = 1$           |
| At inlet                             | $i = 1,$   | $M = 0.80$               |
| For air                              | $k = 1.4,$ | $R = 287. \text{ J/kgK}$ |
| $P_{\text{exit}}/P_{\text{t,inlet}}$ | = 0.85,    | 0.80, 0.75               |

### Results

The variations of static pressure, Mach number, and total pressure for all three back pressures are shown in Fig. 4. All three shocks are captured over four steps. The upstream side of the shock is sharply defined with only minor deviations from the theoretical 1-d solution. On the downstream side, there is a small overshoot and undershoot in static pressure and Mach number over two steps; the total pressure distributions show no overshoots or undershoots and show a sharp decrease over two steps.

### Concluding Remarks

It is hoped that the M&M density interpolation formula will be useful to those organizations like NASA Lewis who are using density-update time-marching codes. It is also hoped that the stability analysis performed under this NASA Grant will be enlightening to users and developers of time-marching codes.

Table 1. Outline of Effective Pressure Method with Different Time Steps - Density Update Scheme.

UNKNOWNNS ( 2 - DIMENSIONS)

$$\rho, u, v, (\rho u), (\rho v), (\rho e_o), h_o, P, T$$

CONTINUITY

$$\frac{\partial \rho}{\partial t} + \nabla \cdot (\rho \underline{u}) = 0 \quad (1)$$

$$\delta \rho = (- \oint (\rho \underline{u}) \cdot d\underline{A}) \delta t_e / \text{Vol}$$

$$\rho = \rho + \delta \rho$$

$$P = \rho RT$$

MOMENTUM (INVISCID)

$$\frac{\partial (\rho \underline{u})}{\partial t} + \nabla \cdot (\rho \underline{u}) \underline{u} = -\nabla p \quad (2)$$

USING EQ. 2 - (u or v) TIMES EQ. 1

$$\rho \delta u = (- \oint (u(\rho \underline{u}) \cdot d\underline{A} + p \underline{i} \cdot d\underline{A}) + u \oint (\rho \underline{u}) \cdot d\underline{A}) * \delta t_m / \text{Vol}$$

$$\rho \delta v = (- \oint (v(\rho \underline{u}) \cdot d\underline{A} + p \underline{i} \cdot d\underline{A}) + v \oint (\rho \underline{u}) \cdot d\underline{A}) * \delta t_m / \text{Vol}$$

$$u = u + \delta u$$

$$v = v + \delta v$$

$$(\rho u) = \rho u$$

$$(\rho v) = \rho v$$

ENERGY

$$h_o = \text{constant}$$

$$T = (h_o - \frac{u^2 + v^2}{2}) / C_p$$



DENTON 1D EXAMPLE

A0= 0

A1= 0

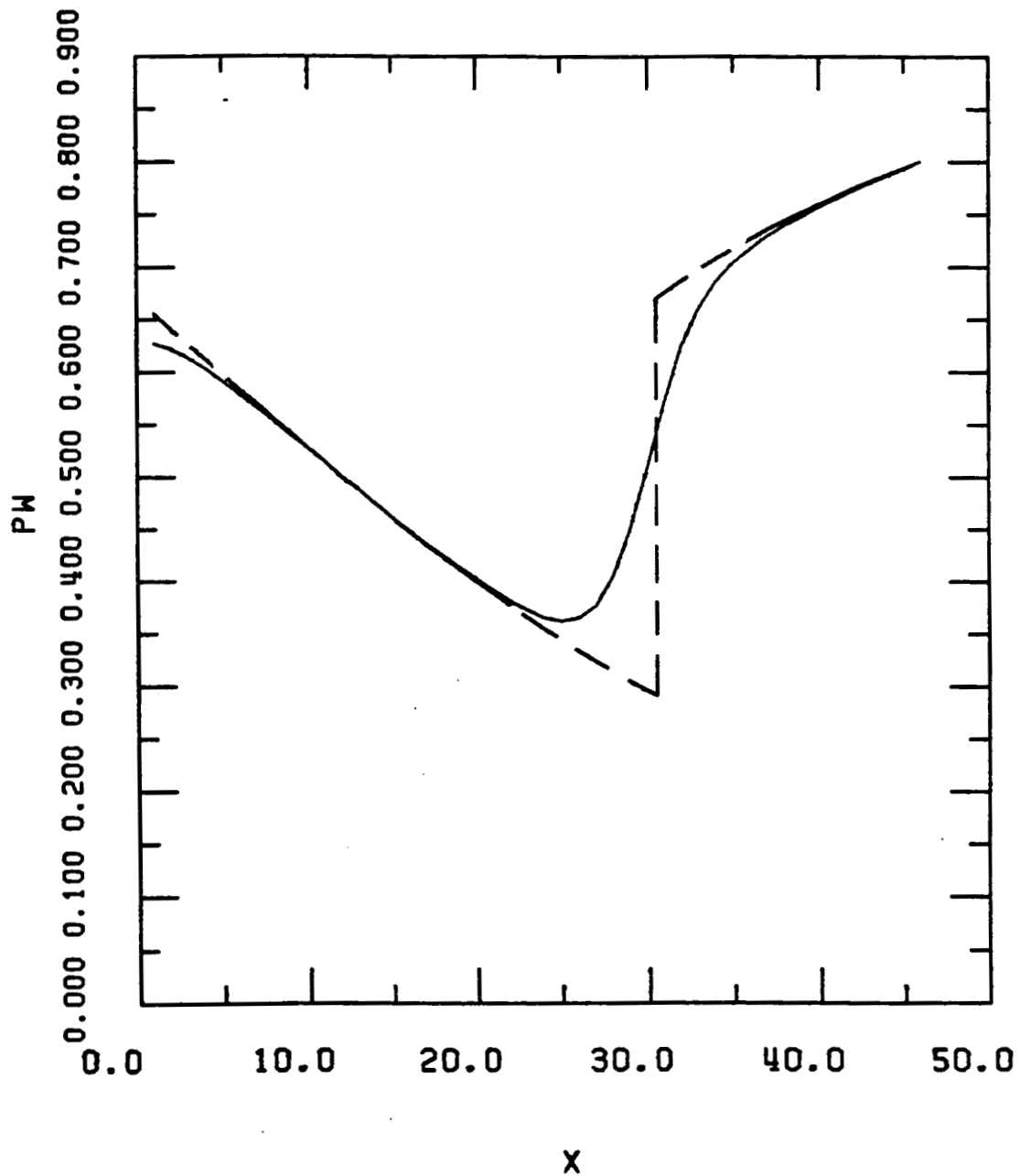


Fig. 1 Comparison of calculated and theoretical 1-D static pressure distributions,  $PW = P/P_{t,inlet}$

— — — theoretical;

— — — calculated using a downwind effective pressure, Eq. 4

Grid spacing,  $\delta x = 1$ ;  $P_{exit}/P_{t,inlet} = 0.80$ .

STABILITY LIMITS,  $a_0 + a_1 = 1$

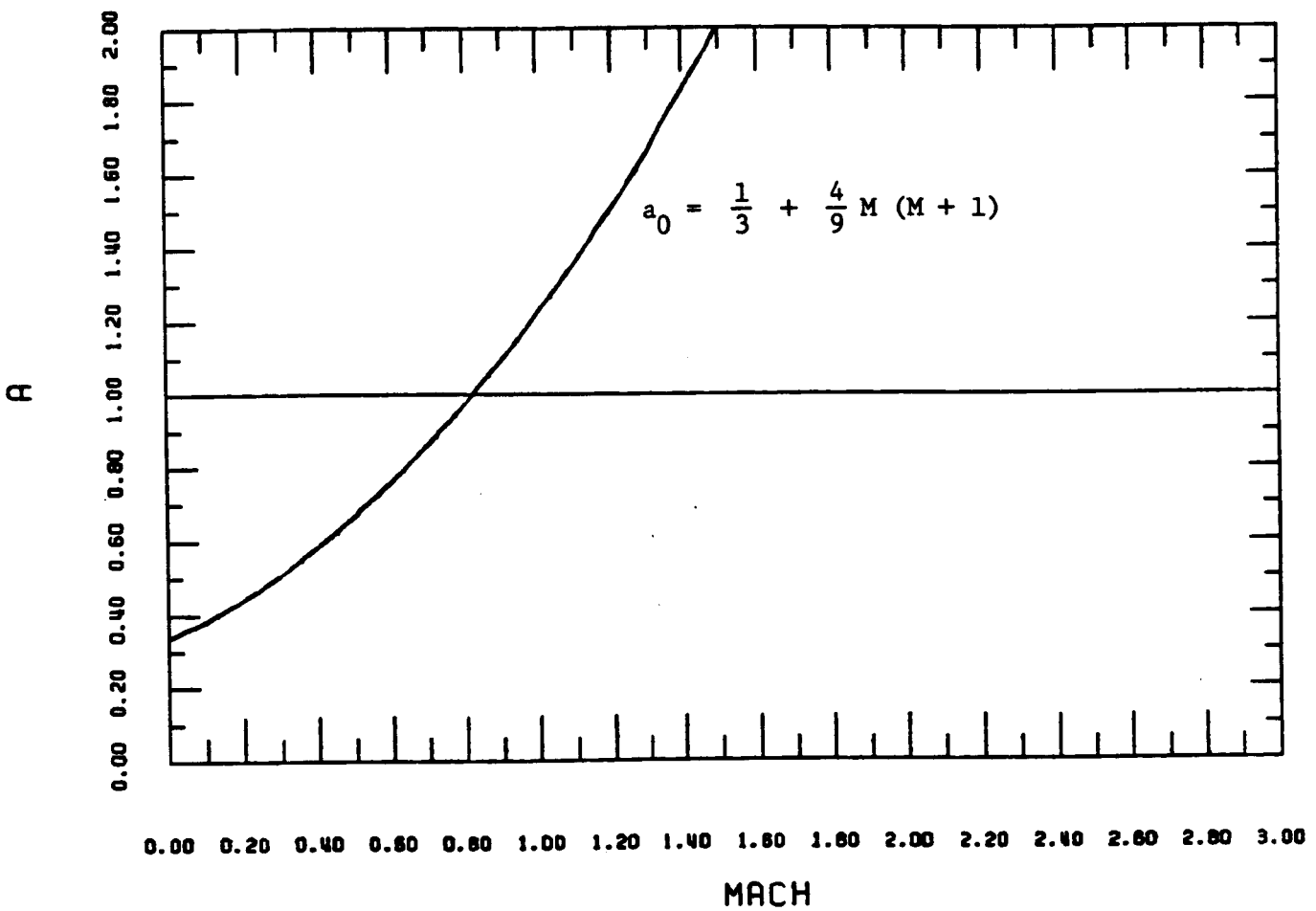


Fig. 2 M & M density interpolation formula for use with Effective Pressure, Density Update, Time Marching Methods.  
Stability limits for  $a_0$  when  $a_2 = 0$  and  $a_0 + a_1 = 1$ .

MACH NUMBER DEPENDENT A'S WITH  $a_0 + a_1 = 1$

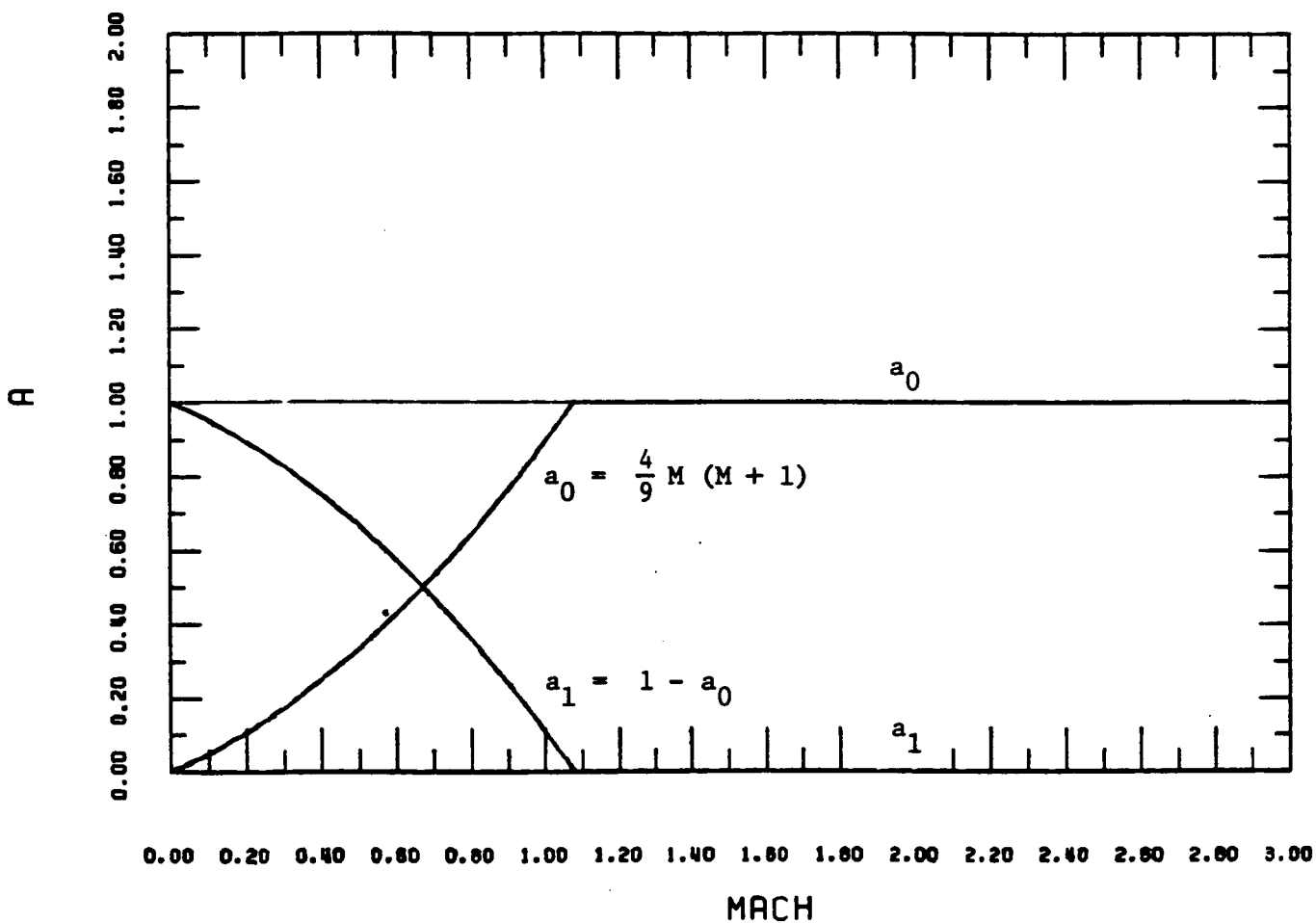


Fig. 3 M & M Mach number dependent values for the density interpolation coefficients,  $a_0$  and  $a_1$ , in the Effective Pressure Method.

DENTON 1D EXAMPLE

$$A0 = M \times (M+1) \times 4/9 \quad A1 = 1 - A0$$

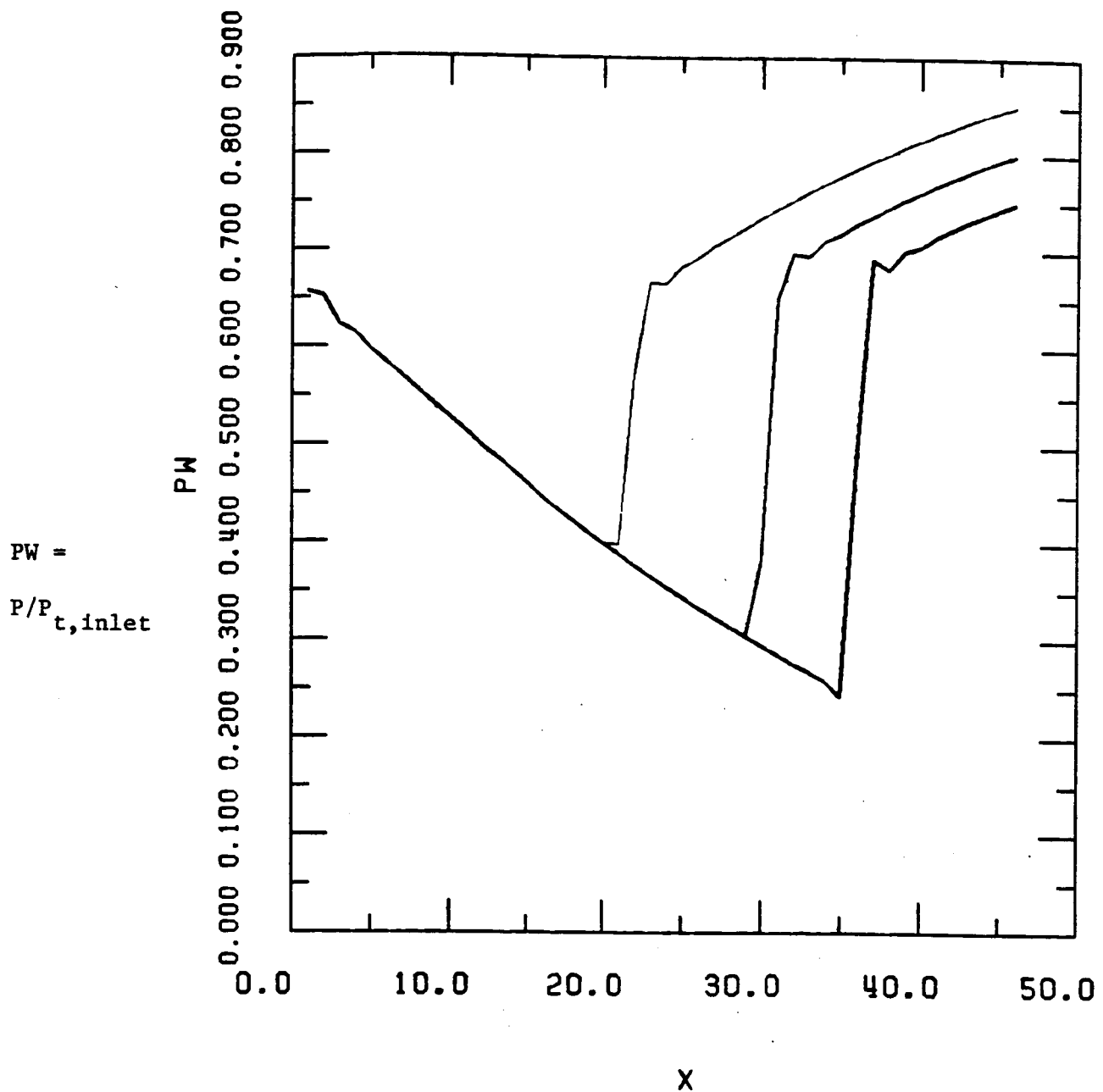


Fig. 4a Calculated 1-D solution for Denton's nozzle using M & M density interpolation formula with the Nicholson/Moore Effective Pressure, Density Update Method.

Calculations for three exit static pressures at  $x = 46.$ ,  
 $P_{\text{exit}}/P_{t,\text{inlet}} = 0.85, 0.80, \text{ and } 0.75.$

DENTON 1D EXAMPLE

$$A0 = M \times (M+1) \times 4/9 \quad A1 = 1 - A0$$

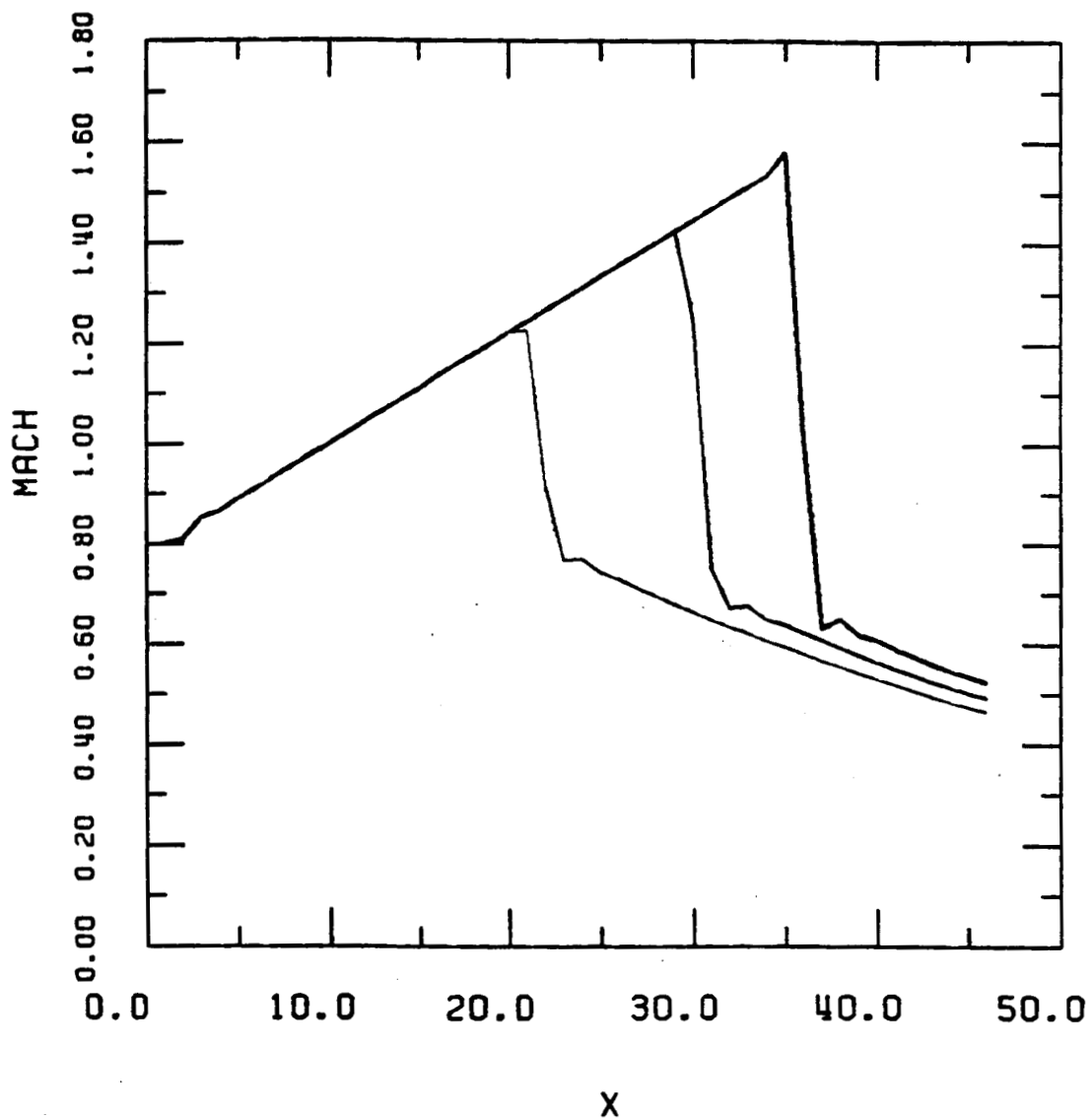


Fig. 4b Mach number.

DENTON 1D EXAMPLE

$$R0 = M \times (M+1) \times 4/9 \quad R1 = 1 - R0$$

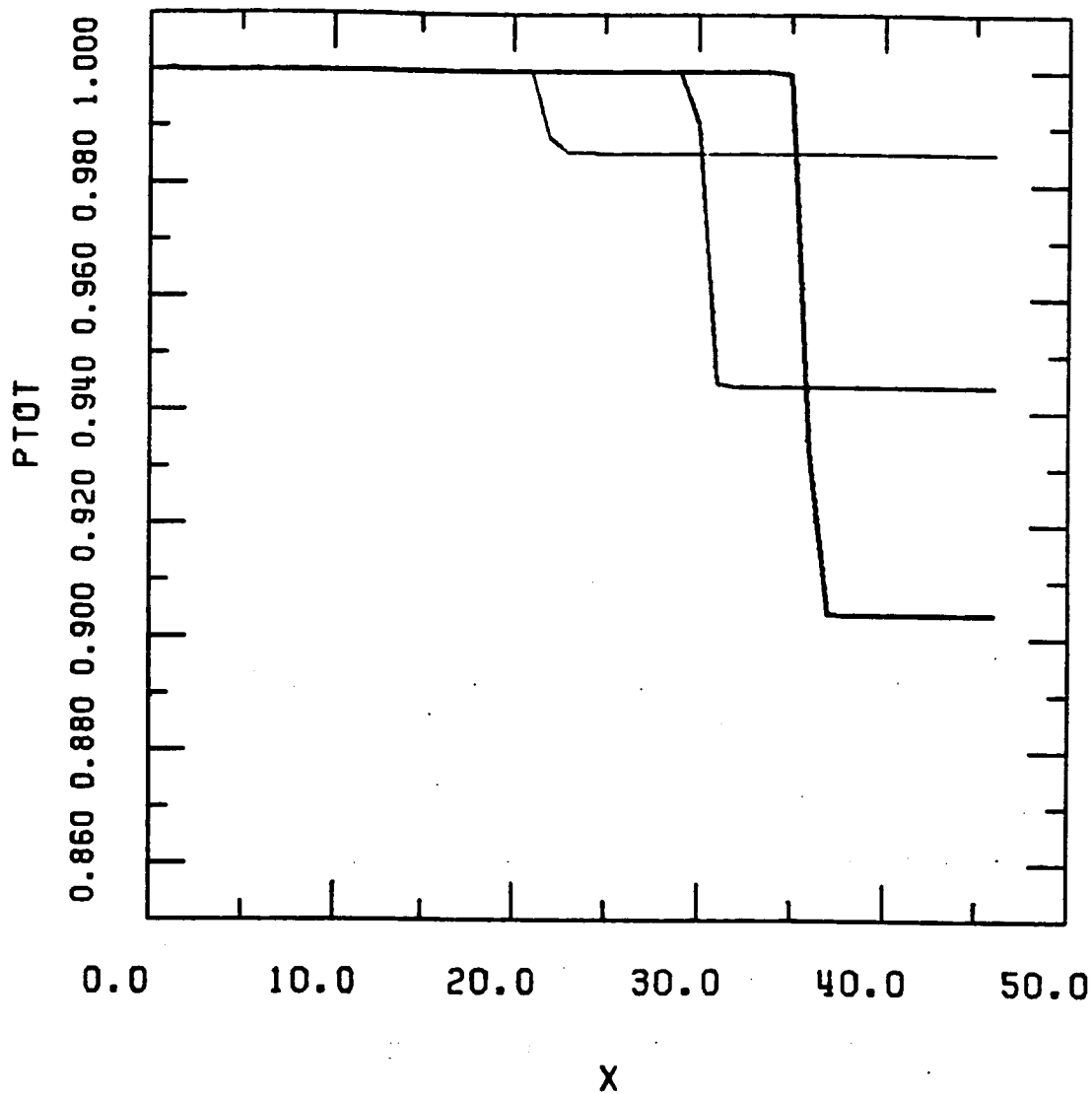


Fig. 4c  $PTOT = P_t / P_{t,inlet}$

APPENDIX A  
TITLE PAGES AND ABSTRACTS OF REPORTS  
prepared in connection with  
NASA GRANT NO. NAG 3-593

Development of a Finite Volume  
Time Marching Method

by  
Stephen Nicholson

February 1985

Turbomachinery Research Group

Report No. JM/85-3

Mechanical Engineering Department  
Virginia Polytechnic Institute and State University  
Blacksburg, Virginia 24061



## DEVELOPMENT OF A FINITE VOLUME TIME MARCHING METHOD

### ABSTRACT

The objective of the current work is to develop and demonstrate a Navier-Stokes approach for transonic flow which includes viscous terms in the finite-volume method. The accuracy of the computational method will be verified using a transonic diffuser as a test case. The computational goal is to calculate the flow in sufficient detail and with sufficient accuracy that the loss generating mechanisms can be studied to assess the sources of inefficiency in the transonic diffuser. The purpose of this report is to document progress made in the development of the time-marching finite-volume method from September 1984 to December 1984.

omit

N85-26712

Semi-Annual Status Report  
on  
NASA Grant No. NAG 3-593

Thermodynamic Evaluation of Transonic Compressor Rotors  
Using the Finite Volume Approach

for the period  
12/20/84 - 5/31/85

by  
Stephen Nicholson  
Instructor  
and  
John Moore  
Professor of Mechanical Engineering  
Principal Investigator

Grantee Institution -  
NASA Lewis Research Center  
21000 Brookpark Road  
Cleveland, Ohio 44135

Turbomachinery Research Group  
Report No. JM/85-6

Mechanical Engineering Department  
Virginia Polytechnic Institute and State University  
Blacksburg, Virginia 24061

EXTENSION OF A FINITE VOLUME EXPLICIT TIME MARCHING METHOD TO  
LAMINAR AND TURBULENT FLOW

ABSTRACT

This report documents progress made in extending the finite volume explicit time marching method to laminar and turbulent flow during the time period from January to May 1985. The work done is under NASA grant NAG 3-593. Previously, extensions had been made to the finite volume method to improve the accuracy of the calculation of total pressure in compressible inviscid flow. These changes are documented in reference 1 . The current work extends these ideas and develops new ideas which allow the calculation of laminar and turbulent boundary layers in internal flows. The method is verified using four test cases with free-stream Mach numbers ranging from .075 to 1.20.

omit

N86-16220

Annual Report on NASA Grant No. NAG 3-593  
Thermodynamic Evaluation of Transonic Compressor Rotors  
Using the Finite Volume Approach

for the period  
12/20/84 - 12/19/85

by  
John Moore  
Professor of Mechanical Engineering  
Principal Investigator

Stephen Nicholson  
Instructor  
and  
Joan G. Moore  
Research Associate

Grantee Institution -  
NASA Lewis Research Center  
21000 Brookpark Road  
Cleveland, Ohio 44135

Turbomachinery Research Group  
Report No. JM/85-11

Mechanical Engineering Department  
Virginia Polytechnic Institute and State University  
Blacksburg, Virginia 24061

## Abstract

Summer research at NASA Lewis Research Center gave the opportunity to incorporate new control volumes in the Denton 3-D finite-volume time-marching code. For duct flows, the new control volumes require no transverse smoothing and this allows calculations with large transverse gradients in properties without significant numerical total pressure losses.

The summer research also pointed to possibilities for improving the Denton code to obtain better distributions of properties through shocks. Much better total pressure distributions through shocks are obtained when the interpolated effective pressure, needed to stabilize the solution procedure, is used to calculate the total pressure. This simple change largely eliminates the undershoot in total pressure downstream of a shock. Overshoots and undershoots in total pressure can then be further reduced by a factor of 10 by adopting the effective density method, developed at VPI&SU, rather than the effective pressure method. Use of a Mach number dependent interpolation scheme for pressure then removes the overshoot in static pressure downstream of a shock.

The stability of interpolation schemes used for the calculation of effective density is analyzed and a Mach number dependent scheme, the M&M formula, is developed. This formula combines the advantages of the correct perfect gas equation for subsonic flow with the stability of 2-point and 3-point interpolation schemes for supersonic flow.

OMIT

N86-26546

Semi-Annual Status Report  
on  
NASA Grant No. NAG 3-593

Thermodynamic Evaluation of Transonic Compressor Rotors  
Using the Finite Volume Approach

for the period  
12/20/85 - 5/31/86

by  
Stephen Nicholson  
Instructor  
and  
John Moore  
Professor of Mechanical Engineering  
Principal Investigator

Grantee Institution -  
NASA Lewis Research Center  
21000 Brookpark Road  
Cleveland, Ohio 44135

Turbomachinery Research Group  
Report No. JM/86-2

Mechanical Engineering Department  
Virginia Polytechnic Institute and State University  
Blacksburg, Virginia 24061

## ABSTRACT

This report documents progress made in refining and improving the finite-volume explicit time marching method (1, 2, and 3) during the time period from January to May 1986. The work is done under NASA grant NAG 3-593. Previously, extension had been made to the finite volume method to

1. improve the accuracy of the calculation of total pressure in inviscid flow (1).
2. extend the method to allow the calculation of laminar and turbulent boundary layers in internal flows (2).
3. improve the shock capturing properties of the method by introducing a Mach number dependent interpolation scheme for the pressure used in the calculating the density (3).

The current work extends these developments by

1. using the new pressure interpolation scheme in two dimensional viscous calculations.
2. including a more complete description of the viscous stresses.
3. introducing a criteria for the transverse upwind differencing which is a function of the ratio of transverse and streamwise mass fluxes.
4. allowing the calculation of internal flow where boundary layers are present on both wall of the duct.

Specifically, this report is broken up into three sections. Section 1 discusses in detail the manner in which the viscous stresses are evaluated in the non-orthogonal, non-uniform grid. Section 2 investigates the convergence and presents results for calculations of laminar flow in a converging duct.

Section 3 presents results for calculations of transonic turbulent flow in a converging-diverging nozzle; the results are compared with Sajben's measurements and calculations by other authors.



omit

N 86-30731

Status Report - August 1986  
on  
NASA Grant No. NAG 3-593  
Thermodynamic Evaluation of Transonic Compressor Rotors  
Using the Finite Volume Approach

Extension of the Finite Volume Method  
to Laminar and Turbulent Flow

by  
Stephen Nicholson  
Instructor

John Moore  
Professor of Mechanical Engineering  
Principal Investigator

Grantee Institution -  
NASA Lewis Research Center  
21000 Brookpark Road  
Cleveland, Ohio 44135

Turbomachinery Research Group  
Report No. JM/86-6

Mechanical Engineering Department  
Virginia Polytechnic Institute and State University  
Blacksburg, Virginia 24061

**Extension of the Finite Volume Method  
to Laminar and Turbulent Flow**

by

**Stephen Nicholson**

**John Moore, Chairman**

**Mechanical Engineering**

**(ABSTRACT)**

A method has been developed which calculates two-dimensional, transonic, viscous flow in ducts. The finite volume, time marching formulation is used to obtain steady flow solutions of the Reynolds-averaged form of the Navier Stokes equations. The entire calculation is performed in the physical domain. The method is currently limited to the calculation of attached flows.

The features of the current method can be summarized as follows. Control volumes are chosen so that smoothing of flow properties, typically required for stability, is not needed. Different time steps are used in the different governing equations to improve the convergence speed of the viscous calculations. A new pressure interpolation scheme is introduced which improves the shock capturing ability of the method. A multi-volume method for pressure changes in the boundary layer allows calculations which use very long and thin control volumes ( length/height  $\cong$  1000). A special discretization technique is also used to stabilize these calculations which use long and thin control volumes. A special formulation of the energy equation is used to provide improved transient behavior of solutions which use the full energy equation.

The method is then compared with a wide variety of test cases. The freestream Mach numbers range from 0.075 to 2.8 in the calculations. Transonic viscous flow in a converging diverging nozzle is calculated with the method; the Mach number upstream of the shock is approximately 1.25. The agreement between the calculated and measured shock strength and total pressure losses is good. Essentially incompressible turbulent boundary layer flow in an adverse pressure gradient is calculated and the computed distribution of mean velocity and shear stress are in good agreement with

the measurements. At the other end of the Mach number range, a flat plate turbulent boundary layer with a freestream Mach number of 2.8 is calculated using the full energy equation; the computed total temperature distribution and recovery factor agree well with the measurements when a variable Prandtl number is used through the boundary layer.

## APPENDIX B

**An Explicit Finite-Volume Time-Marching Procedure  
for Turbulent Flow Calculations**

Stephen Nicholson, Joan G. Moore and John Moore

Mechanical Engineering Department  
Virginia Polytechnic Institute and State University  
Blacksburg, Virginia 24061

## 1. SUMMARY

A method has been developed which calculates two-dimensional, transonic, viscous flow in ducts. The finite-volume, time-marching formulation is used to obtain steady flow solutions of the Reynolds-averaged form of the Navier Stokes equations. The entire calculation is performed in the physical domain.

The features of the current method can be summarized as follows. Control volumes are chosen so that smoothing of flow properties, typically required for stability, is not needed. Different time steps are used in the different governing equations. A new pressure interpolation scheme is introduced which improves the shock capturing ability of the method. A multi-volume method for pressure changes in the boundary layer allows calculations which use very long and thin control volumes (length/height - 1000). The method is then compared here with two test cases. Essentially incompressible turbulent boundary layer flow in an adverse pressure gradient is calculated and the computed distributions of mean velocity and shear stress are in good agreement with the measurements. Transonic viscous flow in a converging diverging nozzle is calculated; the Mach number upstream of the shock is approximately 1.25. The agreement between the calculated and measured shock strength and total pressure losses is good.

## 2. INTRODUCTION

The finite volume method has been used extensively to solve the Euler equations for transonic flow including flow at high Mach numbers. In internal aerodynamics, McDonald [1] was the first investigator to use the time marching finite volume method. Denton [2] extended McDonald's finite-volume

method to three dimensions. Versions of Denton's method have been used in inviscid-viscous interaction programs for turbomachinery calculations [3-5].

The scope of the present work was to extend a finite volume method like that of Denton's to be able to calculate laminar or turbulent flow in ducts. The new method has the capability to calculate subsonic as well as transonic flow.

### 3. GOVERNING EQUATIONS

The unsteady form of the continuity equation, the x-momentum equation, and the y-momentum equation, in integral form, are used to obtain a steady-state solution for flow through 2-dimensional ducts. The ideal gas equation of state, the assumption of constant total temperature, and a Prandtl mixing length turbulence model complete the governing equations needed to solve for the unknown variables  $\rho$ ,  $u$ ,  $v$ ,  $P$ ,  $\mu$ , and  $T$ .

For a finite control volume where we can assign one value of density to the control volume, and for a finite time step,  $\delta t$ , continuity states that,

$$\rho^{n+1} - \rho^n = \delta\rho = -\left[\iint \rho \underline{u} \cdot d\underline{A}\right] \frac{\delta t}{\delta V_{ol}} \quad (1)$$

where the integral is evaluated explicitly at the current time step,  $n$ . In arriving at an expression which relates the pressure change directly to the continuity error, we will assume that changes in temperature are small in comparison to other changes for one time step. Thus, we can relate changes in pressure to changes in density through the ideal gas equation of state,

$$P^{n+1} - P^n = \delta P = -RT \left[\iint \rho \underline{u} \cdot d\underline{A}\right] \frac{\delta t}{\delta V_{ol}} \quad (2)$$

For the method introduced in the current work, a non-conservative form of the unsteady momentum equation is used. The non-conservative form is used because it allows the use of different time steps for the continuity and momentum equations. The differences between the non-conservative and conservative forms of the unsteady momentum equations are associated with the unsteady and convective terms. Specifically, we note that

$$\frac{\partial(\rho \underline{u})}{\partial t} + \nabla \cdot \rho \underline{u} \underline{u} = \rho \frac{\partial \underline{u}}{\partial t} + \rho \underline{u} \cdot \nabla \underline{u} \quad (3)$$

and the right hand side of Eq. (3) can be rewritten as

$$\rho \frac{\partial \underline{u}}{\partial t} + \rho \underline{u} \cdot \nabla \underline{u} = \rho \frac{\partial \underline{u}}{\partial t} + \nabla \cdot \rho \underline{u} \underline{u} - \underline{u} (\nabla \cdot \rho \underline{u}) \quad (4)$$

When the right hand side of Eq. (4) is combined with the pressure and viscous terms, the momentum equation in integral form becomes

$$\begin{aligned} (\underline{u})^{n+1} - (\underline{u})^n = \delta(\underline{u}) = & \left[ -\iint \rho \underline{u} \underline{u} \cdot d\underline{A} + \bar{u} \iint \rho \underline{u} \cdot d\underline{A} \right. \\ & \left. - \iint P \delta_{ij} \cdot d\underline{A} + \iint (\mu \nabla \underline{u} + \overline{\mu \nabla \underline{u}^T} \cdot d\underline{A}) \right] \frac{\delta t}{\delta V_{OI}} \quad (5) \end{aligned}$$

To maintain stability, the properties must be updated in the proper sequence. In the current method, the sequence is

1. update the pressure from the continuity equation;
2. update the velocities from the momentum equation using the new pressure and old velocities and old density;
3. update the density from the ideal gas equation of state;
4. update the temperature from constant total temperature.

#### 4. CONTROL VOLUMES

A new control volume has been introduced for this method. To eliminate the need for smoothing of flow properties, there must be as many control volumes across the duct as there are nodes where these variables are calculated. We need as many equations as unknowns. The control volumes also need to be located so that errors in continuity and momentum can correctly influence the changes in pressure or density and velocity without smoothing. The current control volume accomplishes this and is shown in Fig. 1. When calculating the flux through a streamwise face of an element, the value of the flow properties at the node on that face are used. Linear interpolation is used to obtain the flux on the cross-stream face.

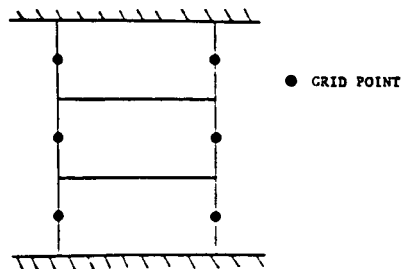


Fig. 1 New Control Volumes

## 5. DISTRIBUTION OF PROPERTIES

The properties at node points are changed in the flow field after each time step because the continuity and momentum equations are not satisfied for a given control volume. A decision must be made about which node, either upstream or downstream, these changes should be allocated to. The criterion used in determining where changes in properties should be sent is that these distributions result in reduced errors in continuity and momentum. The current method uses the following allocation procedure:

1. The pressure is updated through the continuity equation and the pressure change is sent to the upstream node;
2. The u and v velocities are updated through the momentum equations and the changes are sent to the downstream node;
3. The density is updated through the ideal gas equation of state using an interpolated pressure.

## 6. PRESSURE INTERPOLATION PROCEDURE

As part of the updating procedure used by Denton [5], an effective pressure is used in the momentum equations rather than the true thermodynamic pressure determined from the ideal gas equation of state. This effective pressure is needed because if the true pressure is used in the momentum equations the solution may not converge. In the current method, the density used in the continuity and momentum equations is an effective density which may be different than the density obtained using the ideal gas equation of state. This effective density is used to satisfy stability requirements.

Starting with a generalized pressure interpolation equation for the effective density

$$\rho_{I+1} = \left[ P_I + a_0(P_{I+1} - P_I) + a_1 \frac{(P_{I+1} - P_{I-1})}{2} + a_2 \frac{(P_{I+1} - P_{I-2})}{3} \right] \frac{1}{RT_{I+1}}, \quad (6)$$

Mach number limitations were sought for  $a_0$ ,  $a_1$ , and  $a_2$  such that

$$a_1 + a_2 + a_3 = 1 \quad (7)$$

which assures second order accurate solutions. A set of equations for  $a_0$ ,  $a_1$ , and  $a_2$  was chosen which satisfies two stability criteria [6]. The equations are

$$\text{for } M < 2 \quad a_0 = \left(\frac{0.8}{3}\right) \left(\frac{4}{M^2} - 1\right) ; a_1 = 1 - a_0 ; a_2 = 0 :$$

$$\text{for } M > 2 \quad a_0 = 0 ; a_1 = 4/M^2 ; a_2 = 1 - a_1 . \quad (8)$$

These Mach number dependent formulations for  $a_0$ ,  $a_1$ , and  $a_2$  are shown in Fig. 2.

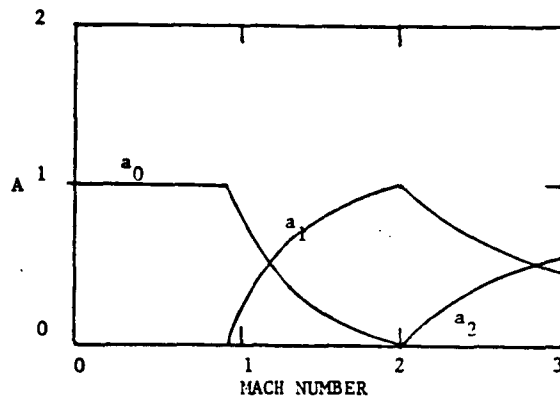


Fig. 2 Mach Number Dependent Values for Coefficients  $a_0$ ,  $a_1$ , and  $a_2$

## 7. TIME STEPS

A unique feature of this method is the use of different time steps for the continuity and momentum equations. Previous workers who have used explicit time marching methods have used the CFL condition as a basis for determining allowable time steps which maintain stability. The same time step is used for both the continuity and momentum equations. In the current method, the expressions that are used to determine the allowable time steps are; for the momentum equations

$$\delta t_m < \frac{1}{\left| \frac{u}{\delta x} \right| + \left| \frac{v_{eff}}{\delta y} \right| + \left| \frac{2\mu}{\rho(\delta y)^2} \right|} \quad (9)$$

and for continuity,

$$\delta t_c < \frac{1}{2RT \left[ \frac{\delta t_m}{(\delta x)^2} + \frac{\delta t_m}{(\delta y)^2} + \left| \frac{u}{RT\delta x} \right| + \left| \frac{v}{RT\delta y} \right| \right]} \quad (10)$$

where  $\delta t_m$  is the momentum time step,  $\delta t_c$  is the continuity time step and  $v_{eff}$  is an effective y-component of velocity. The advantage of using different time steps is that, for low



velocity regions of the flow, the allowable momentum time step can be significantly larger than that allowed by the CFL condition. These larger time steps allow the boundary layer profiles to change more rapidly and enhance the convergence rate significantly compared with a method which uses the CFL condition.

## 8. BOUNDARY CONDITIONS

For viscous flow, at the upstream boundary, the total temperature, freestream total pressure, inlet boundary layer velocity profile, and flow angle are specified. Along the downstream boundary the static pressure is specified. Pressures along the solid boundaries are determined from linear extrapolation. For viscous flow, the values of the x-component and y-component of velocity are set equal to zero at solid walls.

## 9. TURBULENCE MODEL

A Prandtl mixing length model is used to model the turbulent stresses. The model is

$$\mu_{\text{eff}} = \mu_{\ell} + \mu_t \quad \mu_t = \rho L^2 \frac{du}{dy}$$

L is smaller of 0.08 times the width of boundary layer  
or 0.41 times the distance to the wall

Van Driest Correction

$$L = 0.41 "y" (1 - \exp[- "y" \sqrt{\rho\tau}/26 \mu_{\ell}])$$

Near Wall Correction  $\mu_{\text{eff}} = \sqrt{\mu_{\ell} (\mu_{\ell} + \mu_t)}$

## 10. MULTI-VOLUME METHOD FOR PRESSURE CHANGES

Control volumes are grouped in the boundary layer to form a larger global control volume. The continuity error is calculated for this global control volume and changes in pressure are assigned equally to each of the upstream nodes for each control volume making up the global control volume. Then the global control volume is made successively smaller towards the wall. This is shown schematically in Fig. 3. The entire pressure change for one iteration at each node within the multi-volume region is determined by adding together all the pressure changes assigned to that node.

The multi-volume method propagates pressure changes rapidly through the boundary layer and minimizes transverse pressure gradients in the intermediate solution. The above changes allow the calculation of boundary layer flows where

the control volumes near the wall can have aspect ratios (length/height) over 1000.

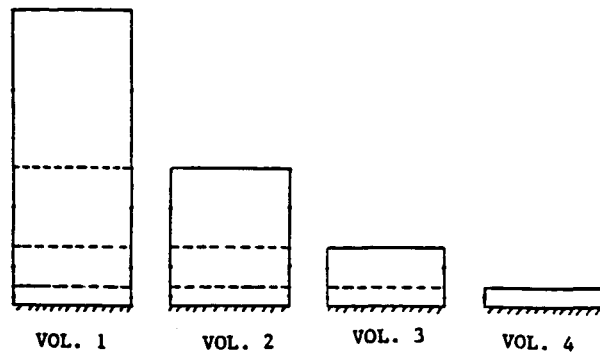


Fig. 3 Multi-Volume Method for Pressure Changes in the Boundary Layer

#### 11. TRANSVERSE UPWIND DIFFERENCING

When the control volumes become long and thin near the wall of the duct, the fluxes through the top and bottom faces of the control volume become more significant in comparison to the fluxes through the streamwise faces. To strengthen the diagonal dominance of the coefficient matrix, the momentum fluxes through the transverse faces may be calculated using interpolated velocities upstream in the transverse direction rather than the actual interpolated values. The interpolation functions and the derivation of the functions is discussed in more detail in Ref. 6.

#### 12. SAMUEL AND JOUBERT INCOMPRESSIBLE TURBULENT BOUNDARY LAYER

Incompressible turbulent boundary layer flow in a diverging duct was calculated for test case 0141 of the Stanford Conference [7]. The grid used in the present calculations is shown in Fig. 4. The inlet velocity is 26 m/s.

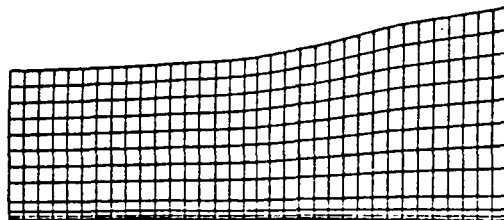
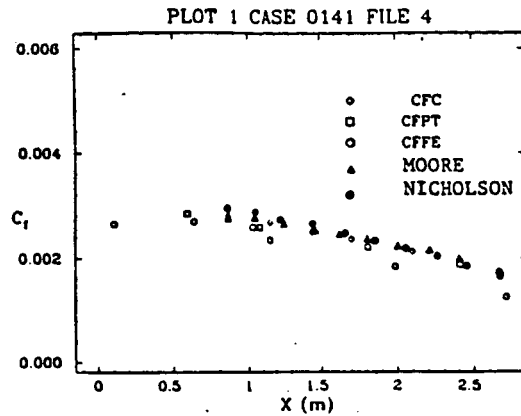


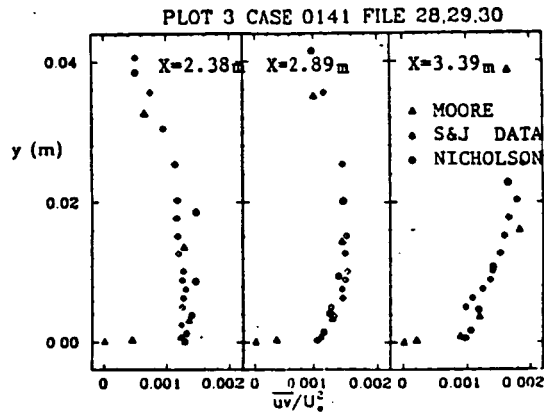
Fig. 4 Geometry and Grid for Samuel and Joubert

Figure 5a shows a comparison of the calculated skin friction coefficient with the experimental results and with the results from the Moore cascade flow program. The agreement is excellent. A comparison of the calculated turbulent shear stress distribution,  $\overline{uv}$ , with the experi-

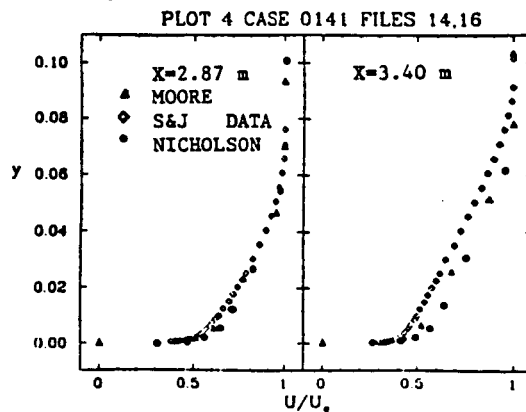
mental results is shown in Fig. 5b. The agreement is good. Figure 5c shows good agreement also between the calculated and measured velocity profiles at two locations in the duct.



5a) Skin Friction Coefficient



5b) Turbulent Shear Stresses



5c) Velocity Profiles

Fig. 5 Results for Samuel and Joubert

### 13. MDRL DIFFUSER CALCULATIONS

The diffuser geometry (Model G) is shown in Figure 6a [8,9]. Figure 6a also shows the computational grid used which has 87 grid points in the axial direction and 20 points across the flow. The inlet boundary layer thicknesses were specified as 9% and 4.5% of the inlet diffuser height for the curved and flat wall boundary layers, respectively. For this calculation, the ratio of exit static pressure to the inlet total pressure was 0.826. In the experiment, this test point results in transonic flow in the diverging portion of the duct with a Mach number of approximately 1.235 upstream of a nearly normal shock, and the flow remained fully-attached throughout the diffuser at this test condition.

A contour plot of static pressure is shown in Fig. 6b. The shock can be seen in the diverging portion of the duct. The shock is well defined as illustrated by the high clustering of contours at the shock. Figure 6c shows a Mach number contour plot for the calculations. The calculated and measured curved wall static pressures are compared in Fig. 7. The shock is well defined and no overshoot occurs in the static pressure.

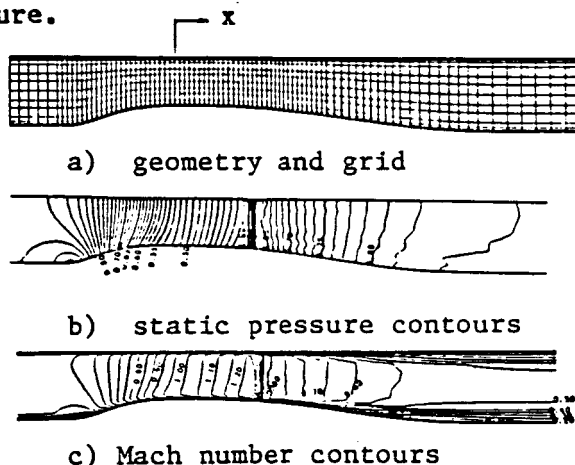


Fig. 6 Geometry and Contours for MDRL Diffuser

Measured shock locations on the curved wall and in the middle of the duct are plotted in Fig. 8 as a function of shock Mach number,  $M_{\sigma u}$ , determined from the minimum wall static pressures on the curved wall. The minimum wall static pressure in the calculation is located at  $x/h = 1.5$ ; this is taken to be the location of the shock. The Mach number upstream of the shock was determined to be 1.256 from the calculated total pressure ratio across the shock in the freestream. This result is plotted in Fig. 8 and it agrees well with the measured shock location. Comparisons of calculated and measured velocity profiles (see Ref. 9) at two axial locations along the duct are shown in Fig. 9. The agreement is good. The mass averaged total pressure at the diffuser exit divided by the inlet freestream total pressure

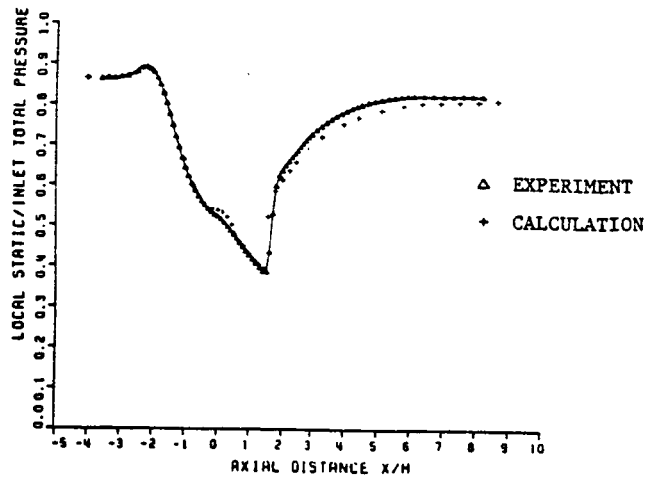


Fig. 7 Curved Wall Static Pressures for MDRL Diffuser

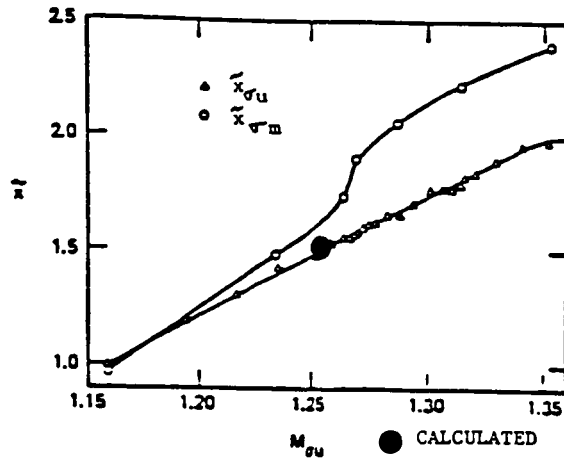


Fig. 8 Comparison of Computed and Measured Shock Position in MDRL Diffuser

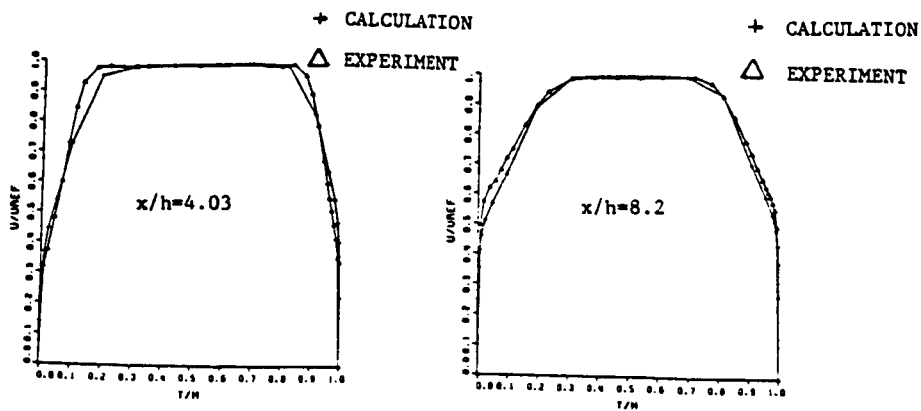


Fig. 9 Velocity Profiles at  $x/h = 4.03$  and  $8.2$  in MDRL Diffuser

is calculated from the numerical results to be 0.9615. This compares well with the measured value of 0.965, obtained from the data of M. Sajben and T. J. Bogar, midway between the diffuser side walls.

The total CPU time for the MDRL diffuser calculations was approximately 35 minutes on an IBM 3031.

#### 14. CONCLUSIONS

An explicit finite volume time marching method has been extended to allow the calculation of laminar and turbulent flow in ducts. Both subsonic and supersonic flow can be calculated with the method. Incompressible turbulent boundary layer flow in an adverse pressure gradient was calculated. The agreement between the calculated and measured skin friction coefficient, turbulent shear stress distribution, and mean velocity profiles was good. Transonic viscous flow through a converging diverging nozzle was calculated. The computed and measured velocity profiles were in good agreement especially near the exit of the nozzle. The computed and measured shock locations were compared and were found to be in good agreement. Viscous and shock losses in the diffuser were well modelled.

#### 15. ACKNOWLEDGMENTS

This work was supported by NASA Lewis Research Center under NASA grant NAG 3-593. The authors are grateful to Jerry R. Wood and Lou A. Povinelli for their encouragement and technical assistance. Miklos Sajben and Thomas J. Bogar kindly provided data on their diffuser tests at the McDonnell Douglas Research Laboratories, in Saint Louis, Missouri.

#### 16. REFERENCES

1. MCDONALD, P. W. - The Computation of Transonic Flow Through Two Dimensional Gas Turbine Cascades. ASME Paper 71-GT-89.
2. DENTON, J. D. - Extension of the Finite Area Time Marching Method to Three Dimensions. VKI Lecture Series 84, Transonic Flow in Axial Turbomachines, February 1976.
3. SINGH, U. K. - A Computation and Comparison with Measurement of Transonic Flow in an Axial Compressor with Shock and Boundary Layer Interaction. ASME Paper 81-Gr/GT-5.
4. CALVERT, W. J. - An Inviscid-Viscous Interaction Treatment to Predict the Blade-to-Blade Performance of Axial Compressors with Leading Edge Normal Shock Waves. ASME Paper 82-GT-135.

5. DENTON, J. D. - An Improved Time Marching Method for Turbomachinery Calculations. ASME Paper 82-GT-239.
6. NICHOLSON, S. - Extension of the Finite Volume Method to Laminar and Turbulent Flow. Ph.D. Thesis, Virginia Polytechnic Institute and State University, Blacksburg, VA, 1986.
7. KLINE, S. J., CANTWELL, B. J., and LILLEY, G. M. - Complex Turbulent Flow Computation-Experiment. 1980-81 AFOSR-HTTM-Stanford Conference on Complex Turbulent Flows, 1982.
8. BOGAR, T. J., SAJBEN, M., and KROUTIL, J. C. - Characteristic Frequency and Length Scale in Transonic Diffuser Flow Oscillations. AIAA Paper 81-1291.
9. SALMON, J. T., BOGAR, T. J., and SAJBEN, M. - Laser Velocimeter Measurements in Unsteady, Separated, Transonic Diffuser Flows. AIAA Paper 81-1197.

## APPENDIX C

Explicit Finite-Volume Time-Marching Calculations  
of Total Temperature Distributions in Turbulent Flow

Stephen Nicholson, Joan G. Moore and John Moore

Mechanical Engineering Department  
Virginia Polytechnic Institute and State University  
Blacksburg, Virginia 24061

## 1. SUMMARY

A method has been developed which calculates two-dimensional, transonic, viscous flow in ducts. The finite volume, time marching formulation is used to obtain steady flow solutions of the Reynolds-averaged form of the Navier Stokes equations. The entire calculation is performed in the physical domain. This paper investigates the introduction of a new formulation of the energy equation which gives improved transient behavior as the calculation converges. The effect of variable Prandtl number on the total temperature distribution through the boundary layer is also investigated.

A turbulent boundary layer in an adverse pressure gradient ( $M = 0.55$ ) is used to demonstrate the improved transient temperature distribution obtained when the new formulation of the energy equation is used. A flat plate turbulent boundary layer with a supersonic freestream Mach number of 2.8 is used to investigate the effect of Prandtl number on the distribution of properties through the boundary layer. The computed total temperature distribution and recovery factor agree well with the measurements when a variable Prandtl number is used through the boundary layer.



## 2. INTRODUCTION

This paper is an extension of the work reported elsewhere in this conference [1]. A review of the features of the new method will be included here but a more complete discussion may be found in references 1 and 2.

The features of the current method can be summarized as follows. Control volumes are chosen so that smoothing of flow properties, typically required for stability, is not needed. Different time steps are used in the different governing equations to improve the convergence speed of the viscous calculations. A multi-volume method for pressure changes in the boundary layer allows calculations which use very long and thin control volumes (length/height = 1000).

## 3. GOVERNING EQUATIONS

The unsteady forms of the continuity equation, the x-momentum equation, the y-momentum equation, and the energy equation, in integral form, are used to obtain steady-state solutions for flow through 2-dimensional ducts. This approach differs from our previous work [1] where the assumption of constant total temperature was used instead of the full energy equation. The ideal gas equation of state and a Prandtl mixing length turbulence model [1] complete the governing equations needed to solve for the unknown variables  $\rho, u, v, P, \mu$ , and  $T$ .

For a finite control volume where we can assign one value of density to the control volume, and for a finite time step,  $\delta t$ , continuity states that,

$$\rho^{n+1} - \rho^n = \delta\rho = -\left[ \iint \rho \underline{u} \cdot d\underline{A} \right] \frac{\delta t}{\delta Vol} \quad (1)$$

where the integral is evaluated explicitly at the current time step,  $n$ . In arriving at an expression which relates the pressure change directly to the continuity error, we will assume that changes in temperature are small in comparison to other changes for one time step. Thus, we can relate changes in pressure to changes in density through the ideal gas equation of state.

$$p^{n+1} - p^n = \delta P = -RT \left[ \iint \rho \underline{u} \cdot d\underline{A} \right] \frac{\delta t}{\delta Vol} \quad (2)$$

For the method introduced in the current work, a non-conservative form of the unsteady momentum equation is used. The non-conservative form is used because it allows the current method to use different time steps for the continuity, momentum, and energy equations. The difference between the non-conservative and conservative forms of the unsteady momentum

equation is associated with the unsteady and convective terms. Specifically, we note that

$$\frac{\partial(\rho \underline{u})}{\partial t} + \nabla \cdot \rho \underline{u} \underline{u} = \rho \frac{\partial \underline{u}}{\partial t} + \rho \underline{u} \cdot \nabla \underline{u} \quad (3)$$

and the right hand side of Eq. 3 can be rewritten as

$$\rho \frac{\partial \underline{u}}{\partial t} + \rho \underline{u} \cdot \nabla \underline{u} = \rho \frac{\partial \underline{u}}{\partial t} + \nabla \cdot \rho \underline{u} \underline{u} - \underline{u} (\nabla \cdot \rho \underline{u}) \quad (4)$$

When the right hand side of Eq. 4 is combined with the pressure and viscous terms, the momentum equation in integral form becomes

$$\begin{aligned} (\underline{u})^{n+1} - (\underline{u})^n = \delta(\underline{u}) = & \left[ -\iint \rho \underline{u} \underline{u} \cdot d\underline{A} + \overline{u} \iint \rho \underline{u} \cdot d\underline{A} \right. \\ & \left. - \iint P \delta_{ij} \cdot d\underline{A} + \iint (\mu \nabla \underline{u} + \mu \overline{\nabla \underline{u}^T}) \cdot d\underline{A} \right] \frac{\delta t}{\delta Vol} \end{aligned} \quad (5)$$

To maintain stability, the properties must be updated in the proper sequence. In the current method, the sequence is:

1. update the pressure from the continuity equation;
2. update the velocities from the momentum equations using the new pressure and old velocities and old density;
3. update the density from the ideal gas equation of state;
4. update the temperature from the energy equation.

#### 4. ENERGY EQUATION

For many calculations of transonic viscous flow, the assumption of constant total temperature will give a sufficient representation of the energy equation in the flow field. By assuming constant total temperature, the computations are less expensive to run and the computer storage requirements are less. The assumption of constant total temperature is usually satisfactory if:

1. an adiabatic wall is assumed in the calculations;
2. no work is done on the fluid at the solid boundaries;
3. the Mach numbers in the flow fields are low enough that total temperature gradients within the boundary layer are small;
4. the Prandtl number is approximately 1.0.

For a Prandtl number of 0.9, the solution should not deviate greatly from the constant total temperature assump-

tion. However for high speed flow, the energy equation should be included in the calculations especially if the Prandtl number deviates greatly from 1.

Two forms of the integral formulation of the energy equation will be derived next.

The energy equation in differential form is

$$\frac{\partial E_t}{\partial t} + \nabla \cdot E_t \underline{u} = -\nabla \cdot \underline{q} + \nabla \cdot [\underline{u} \cdot (\mu \nabla \underline{u} + \mu \nabla \underline{u}^T)] - \nabla \cdot P \underline{u} \quad (6)$$

where the total energy per unit volume,  $E_t$ , is

$$E_t = \rho (e + 1/2 (u^2 + v^2)) = \rho e_t \quad (7)$$

The left hand side of Eq. 6 can be rewritten as

$$\frac{\partial E_t}{\partial t} + \nabla \cdot E_t \underline{u} = \frac{\partial (\rho e_t)}{\partial t} + \nabla \cdot \rho e_t \underline{u} \quad (8)$$

and

$$\frac{\partial (\rho e_t)}{\partial t} + \nabla \cdot (\rho e_t) \underline{u} = \rho \frac{\partial e_t}{\partial t} + \rho \underline{u} \cdot \nabla e_t \quad (9)$$

then, expanding the right hand side of Eq. 9, we get,

$$\rho \frac{\partial e_t}{\partial t} + \rho \underline{u} \cdot \nabla e_t = \rho \frac{\partial e_t}{\partial t} + \nabla \cdot \underline{u} e_t - e_t (\nabla \cdot \rho \underline{u}) \quad (10)$$

The procedure just outlined is identical to what was done to the unsteady and convective terms in the momentum equation (see Eqs. 3,4).

The heat flux vector,  $\underline{q}$ , can be represented as

$$\underline{q} = -k\nabla T \quad (11)$$

Substituting Eqs. 8-11 into Eq. 6, we get

$$\begin{aligned} \rho \frac{\partial e_t}{\partial t} = & -\nabla \cdot \rho \underline{u} e_t + e_t (\nabla \cdot \rho \underline{u}) - \nabla \cdot (-k\nabla T) \\ & + \nabla \cdot [\underline{u} \cdot (\mu \nabla \underline{u} + \mu \nabla \underline{u}^T)] - \nabla \cdot P \underline{u} \end{aligned} \quad (12)$$

The integral form of the energy equation is then

$$\begin{aligned} \rho \frac{\delta e_t}{\delta t} \times \delta Vol = & \\ - \iint \rho \underline{u} e_t \cdot d \underline{A} + \bar{e}_t \iint \rho \underline{u} \cdot d \underline{A} - \iint -k\nabla T \cdot d \underline{A} & \quad (13) \end{aligned}$$

$$+ \iiint [ \underline{u} \cdot (\mu \nabla \underline{u} + \mu \nabla \overline{u^T}) ] \cdot d \underline{A} - \iiint P \underline{u} \cdot d \underline{A}$$

where  $\overline{e}_t$ , is an average value for the control volume. As with the momentum equation, Eq. 13 has a term  $\overline{e}_t \iiint \rho \underline{u} \cdot d \underline{A}$ , which removes the continuity error contribution to the energy error.

This form of the energy equation, when incorporated into the current method, behaved poorly. Initially there were large errors in continuity and momentum and these large errors acted through this energy equation to cause errors in the total energy for a control volume. This interaction was destabilizing.

An alternative form of the energy equation will now be derived. This alternative form has enhanced convergence properties when compared with the above formulation. Briefly, the energy equation is reformulated so that changes in total enthalpy,  $h_t$ , are calculated rather than changes in total energy,  $e_t$ , which was done previously. This allows us to see the terms which cause departures from uniform total temperature - for both the steady state solution and the transient solution.

The total enthalpy can be defined in terms of the total energy and the static temperature

$$h_t = e_t + P/\rho \quad (14)$$

or

$$h_t = e_t + RT \quad (15)$$

Taking the derivative with respect to time and multiplying by the density, we get

$$\rho \frac{\partial h_t}{\partial t} = \rho \frac{\partial e_t}{\partial t} + \rho R \frac{\partial T}{\partial t} \quad (16)$$

The static temperature T can be represented in terms of the total enthalpy and the absolute velocity as

$$T = \frac{h_t}{C_p} - \frac{v^2}{2C_p} \quad (17)$$

Therefore

$$\frac{\partial T}{\partial t} = \frac{1}{C_p} \frac{\partial h_t}{\partial t} - \frac{v}{C_p} \frac{\partial v}{\partial t} \quad (18)$$

Substituting Eq. 18 into Eq. 16, we obtain

$$\rho \frac{\partial e_t}{\partial t} = \frac{\rho}{\gamma} \frac{\partial h_t}{\partial t} + \rho \frac{R}{C_p} v \frac{\partial v}{\partial t} \quad (19)$$

where  $\gamma$  is the ratio of specific heat capacities and  $V$  is the magnitude of the velocity vector. Using equations (19) and (14) to eliminate  $e_t$  from equation (12) we get

$$\frac{\rho}{\gamma} \frac{\partial h_t}{\partial t} = -\nabla \cdot \rho \underline{u} h_t + (h_t - \frac{P}{\rho})(\nabla \cdot \rho \underline{u}) + \nabla \cdot k \nabla T \quad (20)$$

$$+ \nabla \cdot [\underline{u} \cdot (\mu \nabla \underline{u} + \overline{\mu \nabla \underline{u}^T})] - \rho \frac{R}{C_p} V \frac{\partial V}{\partial t}$$

Using  $h_t = C_p T + V^2/2$  and  $k = \mu C_p / Pr$ ,  $k \nabla T$  may be replaced by

$$k \nabla T = \frac{\mu}{Pr} \nabla h_t - \frac{\mu}{Pr} \nabla \left( \frac{V^2}{2} \right) \quad (21)$$

and from continuity we may replace  $\nabla \cdot \rho \underline{u}$  with  $-\partial \rho / \partial t$ .

Therefore the energy equation written as a conservation equation for total enthalpy is

$$\begin{aligned} \frac{\rho}{\gamma} \frac{\partial h_t}{\partial t} = & \underbrace{-\nabla \cdot \rho \underline{u} h_t}_{(I)} + \underbrace{h_t (\nabla \cdot \rho \underline{u})}_{(II)} + \underbrace{\nabla \cdot \frac{\mu}{Pr} \nabla h_t}_{(III)} \\ & + \underbrace{\nabla \cdot \mu \left( 1 - \frac{1}{Pr} \right) \nabla \left( \frac{V^2}{2} \right)}_{(IV)} + \underbrace{\nabla \cdot \mu (\underline{u} \cdot \nabla) \underline{u}}_{(V)} + \underbrace{\frac{P}{\rho} \frac{\partial \rho}{\partial t}}_{(VI)} - \underbrace{\frac{\rho R}{C_p} V \frac{\partial V}{\partial t}}_{(VII)} \end{aligned} \quad (22)$$

Terms I and II when combined give  $-\rho \underline{u} \cdot \nabla h_t$ . Therefore terms I + II and III contain  $h_t$  only in the form  $\nabla h_t$ . Thus, when these are the only important terms in the equation, flow with uniform total temperature at the inlet will retain this uniform total temperature provided that the boundary conditions are consistent with this.

Term IV is a viscous transport term for total enthalpy when the Prandtl number is other than 1. Term V is another viscous transport term. It however contains the expression  $(\underline{u} \cdot \nabla) \underline{u}$  which is the gradient of the velocity in the direction of the velocity; these gradients are usually small compared with other velocity gradients. Since terms IV and V have the form  $\nabla \cdot ( )$ , they are not source terms, rather they can only redistribute the total enthalpy. Terms VI and VII on the other hand have the form of source terms. Relative to the steady state, they are proportional to the continuity error and the momentum error, respectively. We may write them as

$$M = \ell \frac{\partial \rho}{\partial t} + m \frac{\partial V}{\partial t} \quad (23)$$

At the steady state, Eq. 22 becomes

$$0 = -\nabla \cdot \rho \underline{u} h_t + \nabla \cdot \frac{\mu}{Pr} \nabla h_t + \nabla \cdot \mu \left(1 - \frac{1}{Pr}\right) \nabla \left(\frac{v^2}{2}\right) + \nabla \cdot \mu (\underline{u} \cdot \nabla) \underline{u} \quad (24)$$

Therefore we may arbitrarily alter the variables  $l$  and  $m$  in Eq. 23 and the steady form of the energy equation, Eq. 24, will be obtained for converged solutions. The transient behavior of  $h_t$  is improved in the calculation procedure by choosing  $l = m = 0$ , i.e. by omitting the transient source terms in the enthalpy equation.

In integral form then the equation for enthalpy changes is

$$\rho \frac{\delta h_t}{\delta t} \delta Vol = \gamma \left\{ - \iint \rho \underline{u} h_t \cdot d \underline{A} + \bar{h}_t \iint \rho \underline{u} \cdot d \underline{A} + \iint \frac{\mu}{Pr} \nabla h_t \cdot d \underline{A} + \iint \left[ \left( \mu - \frac{\mu}{Pr} \right) \underline{u} \cdot \nabla \underline{u}^T + \mu \underline{u} \cdot \nabla \underline{u} \right] \cdot d \underline{A} \right\} \quad (25)$$

where  $\mu = \mu_l + \mu_t$  and  $\frac{\mu}{Pr} = \frac{\mu_l}{Pr_l} + \frac{\mu_t}{Pr_t}$ .

The time step used for the enthalpy equation is the same as for the momentum equation. If the transient source term  $\frac{P}{\rho} \frac{\partial \rho}{\partial t}$  had been retained in the enthalpy equation, it would have been necessary to link the continuity and energy equation time steps. Omitting this term allows us to use different time steps for the energy equation.

## 5. TEST CASES

Two test cases will be used to explore various aspects of the more complete form of the energy equation, Eq. 25, discussed previously.

### 5.1 Turbulent Boundary Layer in an Adverse Pressure Gradient

The geometry and grid used in this test case are shown in Fig. 1. Flow in this geometry was used in Ref. 1 to test the accuracy of the new computational scheme. In Ref. 1 the velocities in the duct were low enough that the flow could be treated as incompressible. Here, the inlet freestream Mach number was increased to 0.55. The purpose of this test case was to illustrate the advantage of the new formulation of the energy equation.

The static temperatures presented in Fig. 2 are from calculations after 500 iterations. It can be clearly seen that the new formulation, Eq. 25, gives a better transient

solution to the energy equation and it should result in a reduction in the computer time required to reach a steady state solution. Fig. 3 shows the corresponding total temperature profiles for the two formulations of the energy equation.

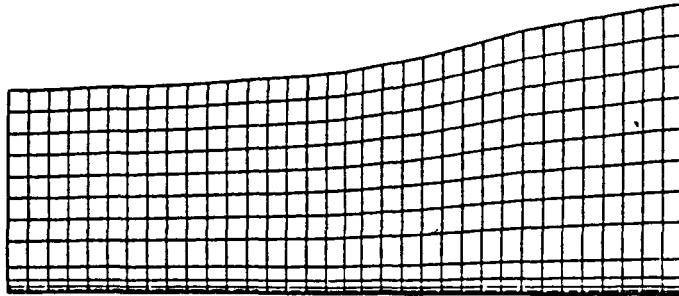


Fig. 1 Grid and Geometry Used to Demonstrate the Advantages of the New Formulation of the Energy Equation

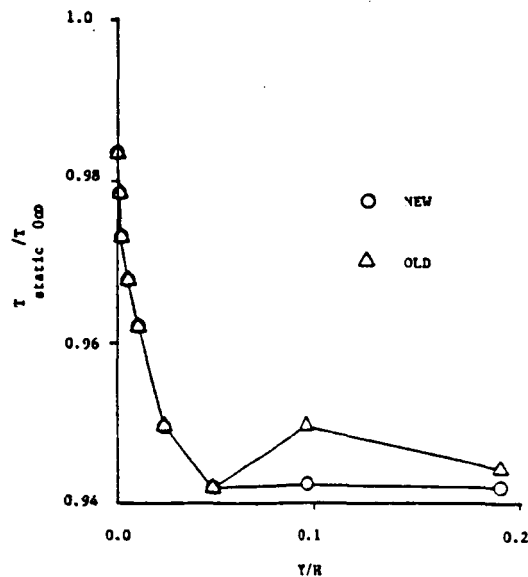


Fig. 2 Static Temperature Distribution Through the Boundary Layer at  $M=0.55$ ,  $x=200$  mm, after 500 iterations

## 5.2 Flat Plate Turbulent Boundary Layer at $M = 2.8$

Van Driest [3] presents the total temperature distribution within a flat plate turbulent boundary layer with a freestream Mach number of 2.8. The experimental total temperature distribution is shown in Fig. 4. The geometry and grid for these calculations are shown in Fig. 5. The height of the duct was 63.5 mm and the length of the duct was 254 mm. The computational grid shown in Fig. 5 consists of 21 axial grid points and 14 transverse grid points. The inlet boundary layer thickness of 6.35 mm was 10% of the duct

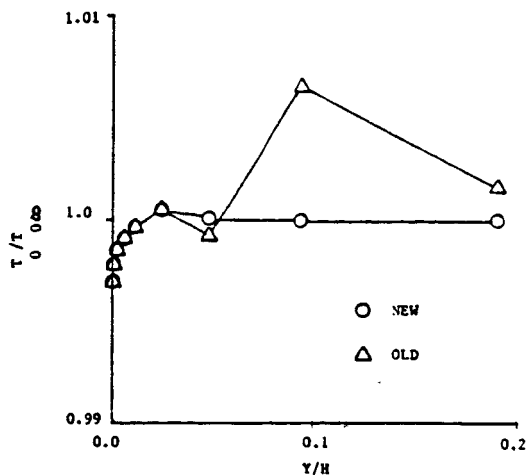


Fig. 3 Total Temperature Distribution Through the Boundary Layer at  $M=0.55$ ,  $x=200$  mm, after 500 iterations

height. The Reynolds number based upon axial distance is approximately  $10^7$ . To stabilize these supersonic flow calculations, the upwind effective density method was used [2]. This means that an effective density used at a grid point is calculated with the ideal gas equation of state using the pressure from the next upstream grid point. The inlet velocity, total temperature, and total pressure were specified at the upstream boundary. Three calculations were performed with different assumptions about the turbulent Prandtl number. These assumptions were

1.  $Pr_t = 0.90$        $Pr_l = 0.73$
2.  $Pr_t = 0.73$        $Pr_l = 0.73$
3.  $Pr_t$  varies linearly through the boundary layer from 0.9 at the wall to 0.66 in the freestream.

The turbulent Prandtl number is typically set equal to a constant of 0.9 in calculations [4]. The calculated total temperature distribution through this boundary layer using a constant turbulent Prandtl number of 0.9 is shown in Fig. 6 (represented as  $\square$ ). The recovery factor is calculated to be 0.920 which compares with the empirically determined value of 0.90. However, the distribution of total temperature through the boundary layer does not compare well with the experiment. If the turbulent Prandtl number is set equal to the laminar Prandtl number of 0.73, the total temperature distribution changes as seen in Fig. 6 (represented at  $\circ$ 's). The distribution through the outer part of the boundary layer has improved but the recovery factor of 0.813 does not compare well with the experimental value of 0.90. Schlichting [5] notes that the turbulent Prandtl number is not constant through the boundary layer. The experiments of H. Ludwig [6] for turbulent flow through a pipe show that the Prandtl number varies from approximately 0.9 at the pipe



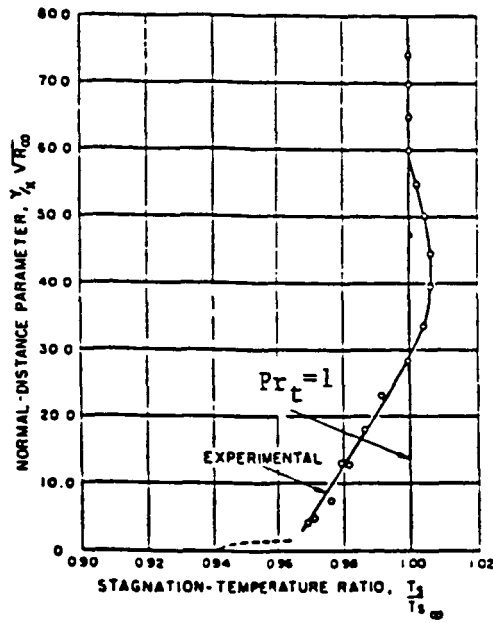


Fig. 4 Experimental Total Temperature Distribution in a Flat Plate Turbulent Boundary Layer  $M=2.8$ ,  $Re_x = 10^7$  after van Driest

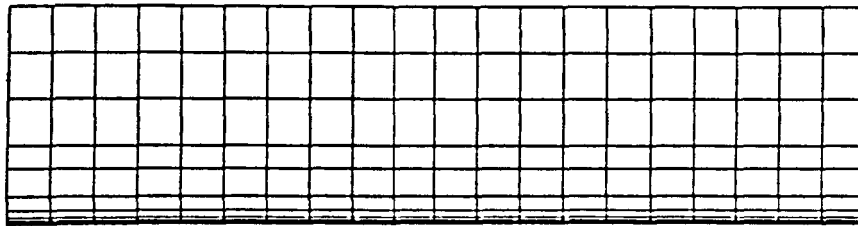


Fig. 5 Geometry and Grid For Boundary Layer Calculations at  $M=2.8$

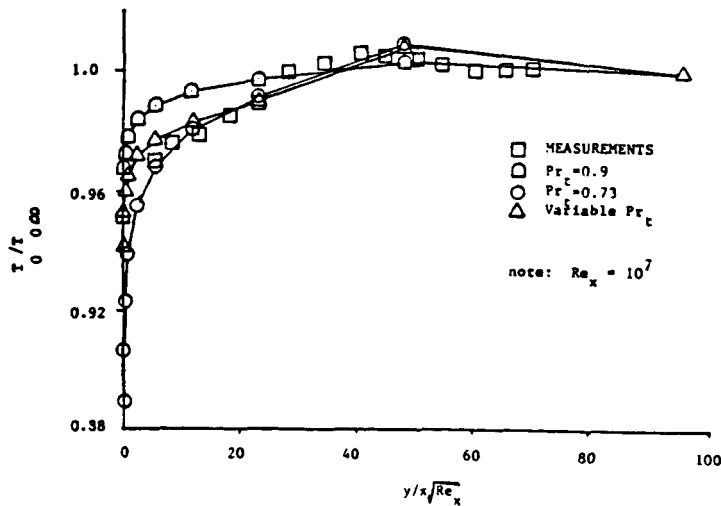


Fig. 6 Total Temperature Distribution For Flat Plate Boundary Layer at  $M=2.8$

wall to 0.66 at the center of the pipe. This distribution is shown in Fig. 7. The variation is almost linear. For the third set of calculations, the Prandtl number was assumed to vary linearly through the boundary layer from 0.9 at the wall to 0.66 at the edge of the boundary layer. The total temperature distribution for this case is shown in Fig. 6 (represented as  $\Delta$ 's). The total temperature distribution calculated using a variable Prandtl number is also compared with the experimental results in Fig. 8. Both the distribution of total temperature through the boundary layer and the recovery factor of 0.90 are in good agreement with the experimentally measured values.

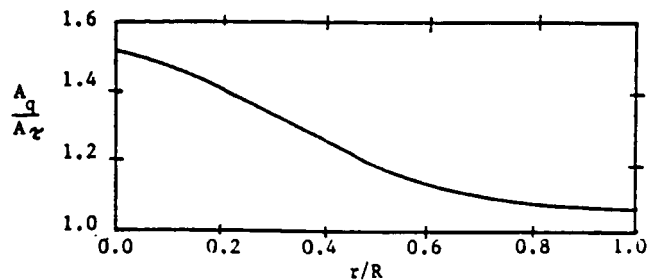


Fig. 7 Ratio of the Turbulent Transfer Coefficient Over the Length of a Radius in Turbulent Pipe Flow

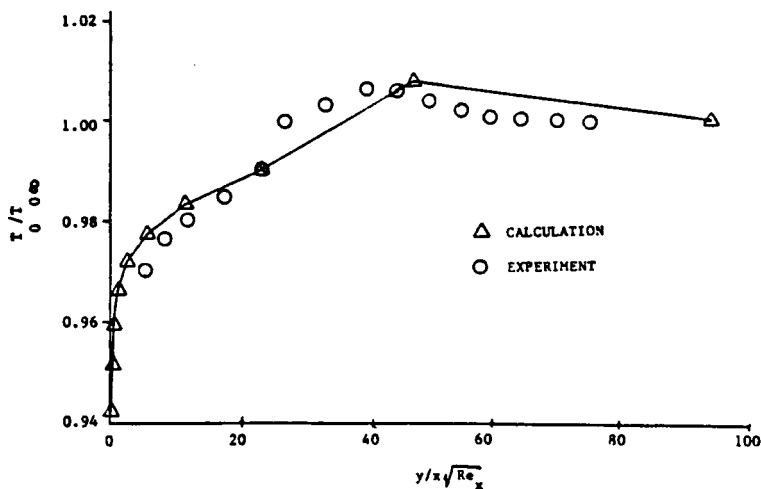


Fig. 8 Total Temperature Distribution For Flat Plate Boundary Layer at M=2.8 Computation vs. Experiment

## 6. CONCLUSIONS

A new formulation for the energy equation was introduced which has improved transient behavior when compared with the standard formulation. The new formulation removes the influences of continuity and momentum errors from the energy equation during transients in the solution.

For flat plate turbulent boundary layer flow with a freestream Mach number of 2.8, the calculated total temperature profile was improved by using a variable Prandtl number through boundary layer. The recovery factor of 0.90 agreed very well with the empirically determined value of 0.9.

## 7. ACKNOWLEDGEMENTS

This work was supported by NASA Lewis Research Center under NASA Grant NAG 3-593. The authors are grateful to Jerry R. Wood and Lou A. Povinelli for their encouragement and technical assistance.

## 8. REFERENCES

1. NICHOLSON, S., MOORE, J. G., and MOORE, J. - Extension of the Finite Volume Time Marching Method to Laminar and Turbulent Flow. 5th International Conference on Numerical Methods in Laminar and Turbulent Flow. July 6-10, 1987, Montreal, Canada.
2. NICHOLSON, S. - Extension of the Finite Volume Method to Laminar and Turbulent Flow. PhD thesis Virginia Polytechnic Institute and State University, Blacksburg, VA, 1986.
3. VAN DRIEST, E. R. - Turbulent Boundary Layer in Compressible Fluids, Journal of the Aeronautical Sciences, Vol. 18, No. 3, March 1951.
4. ANDERSON, D. A., TANNEHILL, J. C., and PLETCHER, R. H. - Computational Fluid Mechanics and Heat Transfer, Hemisphere Publishing Company, 1984.
5. SCHLICHTING, H. - Boundary Layer Theory, Sixth Edition, McGraw-Hill, 1968.
6. LUDWIG, H. - Bestimmung des Verhältnisses der Austauschkoefizienten für Wärme und Impuls bei turbulenten Grenzschichten. ZFW, 73-81, 1956.